DM

Development of New Nanocomposites for Waste Water Cleaning

MASTER DISSERTATION

UNIVERSIDADE da MADEIRA
A Nossa Universidade
www.uma.pt

July | 2019

Development of New Nanocomposites for Waste Water Cleaning

MASTER DISSERTATION

Sabriie Vatansever
MASTER IN NANOCHEMISTRY AND NANOMATERIALS

SUPERVISOR
Gianaurelio Cuniberti

CO-SUPERVISOR
João Manuel Cunha Rodrigues
Nadia Licciardello

Development of New Nanocomposites for Waste Water Cleaning

Dissertation submitted to the University of Madeira in fulfilment of the requirements for the degree of Master in Nanochemistry and Nanomaterials

By Sabriie Vatansever

Work developed under the supervision of Professor Gianaurelio Cuniberti and co-supervised by Professor João Manuel Cunha Rodrigues and Dr. Nadia Licciardello

Faculdade de Ciências Exatas e de Engenharia

Centro de Química da Madeira

Campus Universitário da Penteada

Funchal-Portugal

July 2019

Declaration

I hereby declare that this thesis is the result of my own work, is original and was written by me. I also declare that its reproduction and publication by Madeira University will not break any third-party rights and that I have not previously (in its entirety or in part) submitted it elsewhere for obtaining any qualification or degree. Furthermore, I certify that all the sources of information used in the thesis were properly cited.

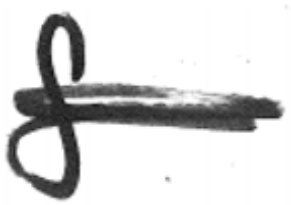

Funchal, 4th of July 2019

To my parents (Nefide & Galip) and

my sister (Sinem)

Acknowledgments

The amazing experience started in 2017, when I got accepted to the master degree in "Nanochemistry and Nanomaterials" at Madeira University, Madeira Island, Portugal. When I came to Madeira, I had fear, passion and, curiosity in my heart which lead me in my academic life. In my academic way, I met great people who helped me to enter into the science world. At the end of my journey, I would like to thank you, *obrigado*, *danke*, *teşekkürler* to who helped me to be a scientist. Now, I would like to say thank you and to show my gratitude to:

First of all, I would like to say a thank to my dear family for their material and spiritual support. Thank you, mom, for pushing me to break the limits and encouraging me all the time. Thank you, dad, for trusting me without any doubts. Thank you, my sister, for believing me that I will success it.

I thank my co-supervisor Prof. Dr. João Rodrigues from ***Centro de Química da Madeira (CQM)*** for his support and supervision. I thank ***Universidade da Madeira (UMa)*** professors and staff that made the biggest difference in my academic life. I thank my great classmates Lydia and Yu in ***Universidade da Madeira (UMa)*** who are always kind and helpful. It was wonderful studying interdisciplinary courses in an intercultural environment.

I would like to thank the ERASMUS+ program for providing me financial supports in ***Dresden Technische Universität Dresden (TUD).***

Many thanks to the ***Chair of Materials Science and Nanotechnology of TUD*** that hosted me for the 8 months in which I prepared my master thesis. Firstly, I would like to thank my first supervisor, Prof. Dr. Gianaurelio Cuniberti, for his collaboration and for providing me all the facilities in the laboratory.

I would like to thank deeply to my second supervisor Dr. Nadia Licciardello for her supervision, motivation and patience and help during my master thesis and her feedback. Without her input and output during my master thesis and reviewing process, this thesis would not have been possible.

To Jiao Wang for helping me in the lab, all the extra time used in teaching me methods, characterization techniques, for sharing her knowledge with me about polymers. With her help, I could understand better about adsorption and polymers. For her extra time and positive attitude, she helped me a lot.

Many thanks to Grit and Sylvi for helping me with the bureaucratic documents.

To my best friends Sıdıka and Ayşe, thank you for supporting me from your hearts.

Thank you!

Teşekkürler!

Financial and scientific support

This work was financially and scientifically supported by:

The Erasmus+ Programme (*European Community Action Scheme for the Mobility of University Students*), University of Madeira (UMa) for providing financial support.

Master in Nanochemistry and Nanomaterials (University of Madeira) for supporting me to spend a research period in TU Dresden.

I acknowledge the host institution Dresden Technical University, Chair of Materials Science and Nanotechnology for hosting me 8 months and providing me required chemicals and devices.

I acknowledge the assistance provided by the Research Infrastructure NanoEnviCz, supported by the Ministry of Education, Youth and Sports of the Czech Republic under Project No. LM2015073.

Abstract

Dyes are one of the most common pollutants in water. In particular, azo dyes are highly toxic, have a complex structure and are particularly hard to degrade because they contain nitrogen-nitrogen double bonds. In addition, in waste water differently charged dyes can be present. Removing these pollutants with a single method or material is hard by using traditional treatment techniques. In this thesis, new nanocomposites were prepared by combining Fe_3O_4/P(NIPAM-*co*-MAA) polymeric microspheres and different generations of Polyamidoamine (PAMAM) dendrimers. The prepared nanocomposites are able to remove differently charged dyes, including the very resistant azo-dye methyl orange, and can also be recycled thanks to their magnetic properties. Different generations (3^{rd}, 4^{th} and 5^{th}) of PAMAM dendrimers and Fe_3O_4/P(NIPAM-*co*-MAA) microspheres have been used in order to synthesize the nanocomposites. The most promising nanocomposites were synthesized by also using a different molar ratio of polymer/dendrimer. All the obtained nanocomposites were tested to adsorb differently charged dyes and, in particular, the positively charged dye basic fuchsin (BF) and the negatively charged azo-dye methyl orange (MO). According to the results, the nanocomposite containing the 5^{th} generation of PAMAM showed the maximum adsorption capacity in the removal of both BF and MO. The adsorption capacity of this nanocomposite towards MO is better than the not grafted polymeric microspheres that can adsorb perfectly BF but cannot adsorb MO. Due to their magnetic properties, the nanocomposites can also be removed by applying an external magnetic field.

Keywords: Methyl Orange; Basic Fuchsin; Adsorption; PAMAM Dendrimer; Fe_3O_4/P(NIPAM-*co*-MAA) microspheres; Reusability

Resumo

Os corantes são um dos poluentes mais comuns na água. Em particular, os corantes azo são altamente tóxicos, têm uma estrutura complexa e são particularmente difíceis de degradar porque contêm ligações duplas azoto-azoto. Além disso, nas águas residuais podem estar presentes corantes de diferentes tipos e cargas. Remover esses poluentes com um único método ou material é difícil usando as técnicas de tratamento tradicionais. Nesta tese, novos nanocompósitos foram preparados combinando microesferas poliméricas de Fe_3O_4/P(NIPAM-*co*-MAA) e diferentes gerações de dendrímeros de poliamidoamina (PAMAM). Os nanocompósitos preparados foram capazes de remover corantes com cargas diferentes, incluindo o muito resistente corante azo-metílico, e também serem reciclados graças às suas propriedades magnéticas. Diferentes gerações de dendrímeros PAMAM (3ª, 4ª e 5ª) e microesferas Fe_3O_4/P(NIPAM-*co*-MAA) foram usadas na preparação dos novos nanocompósitos. Os nanocompósitos mais promissores foram sintetizados utilizando-se diferentes proporções molares de polímero / dendrímero. Todos os nanocompósitos obtidos foram testados para adsorver corantes com diferentes cargas e, em particular, o corante carregado positivamente fucsina básica (BF) e o azo-corante alaranjado de metilo negativamente carregado (MO). De acordo com os resultados obtidos, o nanocompósito contendo a 5ª geração de PAMAM apresentou a capacidade máxima de adsorção na remoção de ambos os corantes, BF e MO. A capacidade de adsorção deste nanocompósito para MO é melhor do que as microesferas poliméricas sozinhas que adsorvem perfeitamente BF, mas não adsorvem o MO. Devido às suas propriedades magnéticas, os nanocompósitos também podem ser reciclados pela aplicação de um campo magnético externo.

Palavras chave: Alaranjado de metilo; Fucsina Básica; Adsorção; Dendrímero PAMAM; Microesferas de Fe_3O_4/P(NIPAM-*co*-MAA); Reciclagem

Table of Contents

Acknowledgments i

Financial and scientific support iii

Abstract v

Resumo vii

Table of Contents ix

List of Figures xi

List of Tables xiii

List of acronyms, abbreviations and symbols xiv

1. Introduction 3

1.1 Environmental and health impact of dyes 5

1.2 Water treatment methods 7

1.3 Adsorption for wastewater treatment 7

1.4 Adsorption of dyes with microspheres 11

1.5 PAMAM dendrimers and their applications in waste water treatment 12

1.6 Objectives 16

2. Materials and methods 21

2.1 Preparation of the PAMAM dendrimer-grafted Fe_3O_4/P(NIPAM-*co*-MAA) nanocomposites 21

2.1.1 Materials 21

2.1.2 Synthetic route for the preparation of the nanocomposites 21

2.2 Characterization of the PAMAM dendrimer-grafted Fe_3O_4/P(NIPAM-*co*-MAA) nanocomposites 22

2.2.1 Instruments used 22

2.3 Adsorption experiments procedure 23

2.3.1 Materials and methodologies 23

2.3.2 Experimental pathway for the adsorption experiments 23

2.4 Working Principles of the instruments used 24

2.4.1 UV-Vis spectroscopy 24

2.4.2 FTIR (Fourier Transform Infrared) spectroscopy 26

2.4.3 DLS (Dynamic Light Scattering) 27

2.4.4 HR-TEM (High-Resolution Transmission Electron Microscopy) 28

3. Results and discussion 31

3.1 Preparation and Characterization of the PAMAM dendrimer-grafted Fe_3O_4/P(NIPAM-*co*-MAA) nanocomposites 31

3.1.1 Synthesis of the nanocomposites 31

3.1.2 ATR-FTIR spectra of the PAMAM dendrimer-grafted Fe_3O_4/P(NIPAM-*co*-MAA) nanocomposites 32

3.1.3 DLS spectra of the PAMAM dendrimer-grafted Fe_3O_4/P(NIPAM-*co*-MAA) nanocomposites 34

3.1.4 UV-Vis spectra of the PAMAM dendrimer, Fe_3O_4/P(NIPAM-*co*-MAA) microspheres and the PAMAM dendrimer-grafted Fe_3O_4/P(NIPAM-*co*-MAA) nanocomposites 35

3.1.5 HR-TEM images of the Fe_3O_4/P(NIPAM-*co*-MAA) microspheres and the PAMAM dendrimer-grafted Fe_3O_4/P(NIPAM-*co*-MAA) nanocomposites 36

3.2 Calculation of amino and carboxylic groups for the nanocomposite preparation 38

3.3 Application: Adsorption of dyes with the PAMAM dendrimer-grafted Fe_3O_4/P(NIPAM-*co*-MAA) nanocomposites 38

3.3.1 Adsorption of basic fuchsin 38

3.3.2 Adsorption of methyl orange 40

3.3.3 Adsorption of basic fuchsin and methyl orange with the PAMAM (G5) grafted-magnetic Fe_3O_4/P(NIPAM-*co*-MAA) nanocomposite and comparison between all nanocomposites 41

4. Conclusions 49

5. References: 53

APPENDIX 63

List of Figures

Figure 1 - Water pollution due to dyes in Bangladesh 4

Figure 2 - Structural formula of basic fuchsin 6

Figure 3 - Structural formula of methyl orange 6

Figure 4 - Fundamental terms of adsorption process 8

Figure 5 - A schematic representation of magnetic separation 10

Figure 6 - Schematic structure of NIPAM, MAA and Fe_3O_4/P(NIPAM-*co*-MAA) microsphere ... 12

Figure 7 - Schematic structure of PAMAM dendrimer 13

Figure 8 - Simplified structure of PAMAM(G3), PAMAM(G4) and PAMAM(G5) dendrimer 14

Figure 9 - Water treatment by dendrimer enhanced filtration process 14

Figure 10 - Variation of total amount of adsorbed Pb^{2+} ions onto different surfaces versus ions concentration in water 15

Figure 11- Removal efficiency by PAMAM (G3) in different pH values and at different initial dye concentrations 16

Figure 12 - A schematic diagram of a UV-Visible setup 25

Figure 13 - A schematic diagram of a FTIR setup 26

Figure 14 - A schematic diagram of a DLS setup 27

Figure 15 - A schematic diagram of a TEM setup 28

Figure 16 - A schematic representation of the reaction of preparation of the PAMAM dendrimer-grafted Fe_3O_4/P(NIPAM-*co*-MAA) nanocomposites 32

Figure 17 - ATR- FTIR spectra of PAMAM (G3), Fe_3O_4/P(NIPAM-*co*-MAA) microspheres and $G3_1P_1$ nanocomposite 33

Figure 18 - ATR- FTIR spectra of PAMAM (G4), Fe_3O_4/P(NIPAM-*co*-MAA) microspheres and $G4_1P_1$ nanocomposite 33

Figure 19 - ATR- FTIR spectra of PAMAM (G5), Fe_3O_4/P(NIPAM-*co*-MAA) microspheres and $G5_1P_1$ nanocomposite nanocomposites 34

Figure 20 - DLS of a) Fe_3O_4/P(NIPAM-*co*-MAA) microspheres, b) $G3_1P_1$, c) $G4_1P_1$ and d)$G5_1P_1$ nanocomposites 35

Figure 21 - UV-Vis spectra of a) PAMAM dendrimers, b) Fe_3O_4/P(NIPAM-*co*-MAA) microspheres c) $G3_1P_1$, $G4_1P_1$ and $G5_1P_1$ nanocomposites 36

Figure 22 - a) HR-TEM image for Fe_3O_4/P(NIPAM-*co*-MAA) microspheres, b) HR-TEM mapping image of Fe_3O_4/P(NIPAM-*co*-MAA) microspheres 37

Figure 23 - a) HR-TEM image for $G4_1P_1$, b) HR-TEM mapping image of $G4_1P_1$..... 37

Figure 24 - UV-Vis spectra of BF in water at different times of the adsorption experiment with a) Fe_3O_4/P(NIPAM-*co*-MAA) microspheres, b) $G3_1P_1$, c) $G4_1P_1$ and d) $G5_1P_1$ nanocomposites 39

Figure 25 - UV-Vis spectra of MO in water at different times of the adsorption experiment testing by a) Fe_3O_4/P(NIPAM-*co*-MAA) microspheres, b) $G3_1P_1$,c) $G4_1P_1$,and D) $G5_1P_1$ nanocomposites 41

Figure 26 - UV-Vis spectra of BF in water at different times of the adsorption experiment testing by $G5_1P_{05}$, $G5_1P_{08}$ nanocomposites 42

Figure 27 - UV-Vis spectra of MO in water at different times of the adsorption experiment testing by $G5_1P_{05}$, $G5_1P_{08}$ nanocomposites..... 42

Figure 28 - Adsorption vs time for a) BF and b) MO when using the nanocomposite $G5_1P_1$..... 43

Figure 29 - Pseudo-first-order model fitting for the adsorption of BF by the nanocomposite $G5_1P_1$..... 45

Figure 30 - Pseudo-second-order model fitting for the adsorption of BF by the nanocomposite $G5_1P_1$..... 45

Figure 31 - Pseudo-first-order model fitting for the adsorption of MO by the nanocomposite $G5_1P_1$..... 45

Figure 32 - Pseudo-second-order model fitting for the adsorption of MO by the nanocomposite $G5_1P_1$..... 46

Figure A1 - Absorbance versus time (min) graph of BF 63

Figure A2 - Absorbance versus time (min) graph of MO 63

Figure A3 - Calibration curve of BF 64

Figure A4 - Calibration curve of MO 64

List of Tables

Table 1 - Some application fields and used adsorbents in waste water treatment 8

Table 2 - The amounts of used chemicals, molar ratio between dendrimer's amino groups and polymer's carboxylic groups for each reaction and the different samples' name 22

Table 3 - Correspondence between sample´s name and initial molar ratio between dendrimer´s amino and polymer´s carboxylic groups to prepare the nanocomposites 32

Table 4 - Adsorption percentages of BF and MO by using Fe_3O_4/P(NIPAM-*co*-MAA) microspheres and the nanocomposites 44

Table 5 - Pseudo-first-order and Pseudo-second-order model parameters of adsorption kinetics of BF and MO 46

List of acronyms, abbreviations and symbols

ATR	Attenuated total reflectance
BF	Basic fuchsin
DCC	N,N'-Dicyclohexylcarbodiimide
DMF	Dimethylformamide
DMAP	4-Dimethylaminopyridine
DLS	Dynamic light scattering
FTIR	Fourier transform infrared spectroscopy
Fe_3O_4/P(NIPAM-*co*-MAA)	Magnetic polymeric microspheres
HR-TEM	High-resolution transmission electron microscopy
MAA	Methacrylic acid
MO	Methyl orange
NIPAM	*N* –isopropylacrylamide
PAMAM	Poly(amidoamine)
SEM	Scanning electron microscope/microscopy
UV-Vis	Ultraviolet-visible spectroscopy

Chapter 1

1. Introduction

Nanotechnology is highly employed and has a strong impact in all industrial sectors, e.g. in medicine, electronics, food packaging, textiles, cosmetics, water treatment techniques[1]. Nanotechnology is expected to play a significant role to solve environmental issues such as water, air, and soil pollution[1,2]. For instance, low concentrations of pollutants can be detected and/or removed with nanoscale catalysts, nano-chemical reactors,

and remote detectors[1]. Analysis, removal and detection technologies will be improved and facilitated by nanoscience[1].

Agricultural and urban activities together with the industrial production of plastics, dyes, pharmaceuticals, non-biodegradable products increased enormously the quantity of waste produced[3,4]. This caused huge water, air and soil pollution that has changed Earth's natural balance[1]. At present, the contamination of water, soil, air with toxic substances threatens Earth, humans, animals and plants[1]. Water pollution is of particular interest due to its importance for life and to the scarcity of accessible water sources[5].

Water is the most critical and significant substance to sustain life[1]. The human body contains between 60% and 80% of water[1]. The Earth's surface is covered by 70% of water, but 97% percent is saltwater[6]. 2.5% of all available water on Earth is freshwater that is stored as groundwater and frozen as polar ice[6]. In reality, 0.5 % of the total water is easily available for people to use on Earth[6]. The main sources of fresh water are rivers, lakes, snow, rainwater and groundwater[1]. These sources are susceptible to pollution because of human activities[1]. Water pollution is the contamination of a body of water or water bodies (rivers, oceans, seas, groundwater, aquifers and lakes) usually caused by human activities[5]. Water pollution arises when unwanted waste spreads in a water system and changes the water quality[5]. In this thesis, water pollution and possible nanotechnology solutions are in focus.

Pollution (*pollutionem* is a term from the Latin and means dirt, disgrace and filth) is the introduction in the environment of materials which cause harm to living organisms, human health and Earth[1]. Pollution takes place when a substance is present in the environment in higher concentration than the natural limit and have harmful effects[1]. There are many forms of pollution[1]. Industrial applications, domestic sources, agricultural practices and hospitals are some of the main sources of pollutants in the environment[1].

There are three main water pollution causes: 1) natural sources such as acid effluents, toxic gases from volcanic activity and volcanic places; 2) domestic sources which are laundry wastes

and sewage; 3) industrial wastes that are the major pollution source[5]. Some industrial wastes generate high quantities of toxic chemicals such as metals, acids, heavy metals, textile wastes (e.g. dyes), and pharmaceuticals[5].

There are many kinds of pollutants, such as inorganic chemicals, radioactive substances, plant nutrients, artificial fertilizers, disease-causing agents[5]. The types of pollution can be divided into physical (big solid waste), biological (bacteria, excessive algal blooms) and chemical (dyes, pharmaceuticals, pesticides, metal ions, oil spills)[5]. Each kind of pollution needs different and specific methods for cleaning water[5].

There are varied effects of pollution on aquatic environments[7]. In developing countries, the pollution of drinking water by sewage causes 14,000 deaths per day[8]. Approximately 700 million Indians do not have a proper toilet and almost 1000 kids die because of diarrhoea in India and other countries[8]. Besides, 500 million Chinese have no safe drinking water[8]. Aquatic pollution can definitely change the aquatic life[7,8]. Thus, disease-carrying microorganisms such as bacteria are carried into the water communities as lakes, river and ground water[8].

Besides physical and biological pollution, chemical pollution is the major environmental issue. By developing industry, the use of chemicals, mainly dyes, are increasing. The dyes from the textile industry contaminate water and cause heavy water pollution. Figure 1 shows the water pollution caused by dyes in Bangladesh.

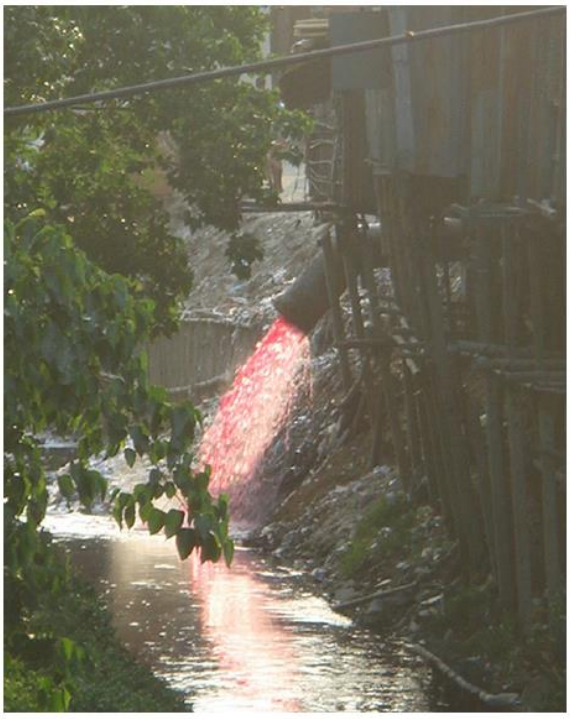

Figure 1: Water pollution due to dyes in Bangladesh[9]

1.1 Environmental and health impact of dyes

All over the world, 800.000 tons of dyes are produced in a year[10]. The textile industry is the biggest producer of dye polluted water[10,11]. Synthetic dyes are used in many industries such as paper printing, textile, food, cosmetics and pharmaceutical[10]. Approximately, 10-15% of synthetic dyes vanish and mix to nature because of the textile industry[10]. Textile processing produces liquid waste, which includes inorganic and organic compounds, which will cause water pollution[10,12]. The amount of wastewater depends on the sort of fabrics manufactured. Roundly, 0.08-0.15 m^3 of water is utilized to obtain 1 kg of textile fabrics[10]. All of these dyes uses are one of the main sources of environmental problems in the last decades[10].

Wastewater is full of chemicals and dyes; some of them are carcinogenic and non-biodegradable being hazardous for human health and the environment[10]. With long term exposure to dyes, there can be probably human health hazards[10]. The dyes cause several health problems like skin, eye, respiratory tract and gastrointestinal irritation[13].

Dyes can stay in the environment and water for a long period because of their photostability and high thermal properties to resist biodegradation[14,15]. The bigger environmental issue with dyes is their absorption and reflection of sunlight by entering the water[14]. The absorption of light reduces the photosynthetic activity of algae, moss and aquatic plants[14,16]. That affects the food chain negatively[14]. The textile dyes in water cut-off the oxygenation capacity of the water and stop sunlight[14,17]. In this way, the photosynthesis process and biological activities stop in aquatic life[18]. Long-time presence of dyes in water causes accumulation in water bodies, aquatic life and fishes[14,19]. Then, the dyes decompose in mutagenic and carcinogenic compounds, and it causes toxicity to life[14,20].

Many wastewater treatment processes as electrodialysis, trickling filters, flocculation, sedimentation, etc. have been used for removing the pollutants from water[21]. Nevertheless, these treatment methods are not effective in removing all chemicals and dyes from wastewater. As a matter of fact, the waste water from textile does not include just a high ratio of dyes, but often also comprise other chemicals such as metal ions[10,22]. Several kinds of trace metals such as Zn, As, Cu and Cr cause health problems such as ulceration of the skin, irritation, nausea, dermatitis, acute tubular necrosis, abdominal pain, vomiting, kidney failure, cancer, bone damage and even death[10,23]. Additionally, textile wastewater also contains microbial and other organic impurities[10].

Water-soluble dyes are hazardous for organisms and especially for liver enzymes[10]. In particular, azo dyes are the largest group of dyes used in the textile industry[10]. Azo dyes have a complex structure and are particularly hard to degrade because they contain nitrogen-nitrogen double bonds (-N=N-) and are highly electron deficient[10,24,25]. Also, azo dyes display carcinogenic effects due to their cleaved products such as aromatic amine groups which induce animal and human tumors[10,25]. These dyes can change the chemical and physical composition of soil, fauna and flora affecting environment and agricultural activity negatively[10]. Even small quantities of azo dyes (<1ppm) are highly visible in water and affect water-gas solubility, transparency and aesthetic appearance[10]. A high concentration of dyes can also cause a decrease of light penetration in water. This can bring to a subsequent reduction of photosynthetic activity and a de-regulation of the biological cycles of aquatic biota with connected oxygen deficiency[10].

The anionic dye Methly Orange (MO) (or Sodium 4-[(4-dimethylamino) phenyl} diazenyl} benzene-1-sulfonate) is a well-known azo-dye. Mostly, MO is used in paper, food and textile industry[10, 9].

Basic Fuchsin (BF) is a poisonous dye which has triphenylmethane group, and it is mostly used in paper, printing, cotton, fibers and industrial production[13,26]. Both BF and MO can affect human health negatively creating issues such as respiratory irritation, nausea, vomiting, Heinz body formation, shock, gastrointestinal irritation and diarrhoea[27,28]. Both BF and MO threaten human health because of their toxicity and carcinogenicity effects[10]. Because of their poor biodegradation, BF and MO cause significant environmental problems and their removal from waste water is a serious topic and should be studied in depth. Figures 2 and 3 show the chemical structure of BF and MO.

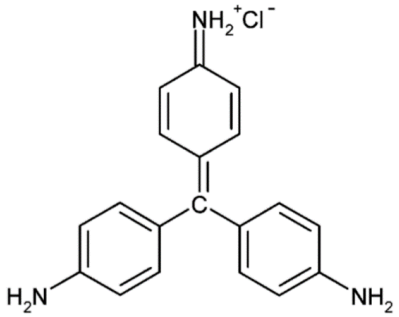

Figure 2: Structural formula of basic fuchsin[26]

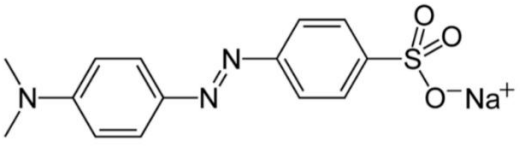

Figure 3: Structural formula of methyl orange[29]

1.2 Water treatment methods

In general, traditional wastewater methods consist mainly of biological and mechanical processes[30]. There are several methods to treat wastewater, such as sedimentation, filtration, aeration, chlorination, and chemical oxidation, microbial and enzymatic decomposition[31]. However, with most of these techniques, it is not possible to remove all pollutants (e.g. traces of dyes or pharmaceuticals) and, therefore, the use of properly engineered nanomaterials is significant in this sense.

Generally, water treatment involves three stages, named primary, secondary and tertiary treatment. In the primary step, coarse solids are removed from wastewater. Then, the rest of the wastewater is transferred to the secondary stage. 90% of the organic pollutants in water are removed by using biological treatment methods such as biofiltration, oxidation ponds and aeration[32]. A tertiary step to remove traces of recalcitrant pollutants, to protect the environment and to improve the effluent quality in water was introduced into the treatment process[30].

In recent years, researchers are studying on removing persistent micropollutants from water, which are not degraded during the treatment process[30]. By developing nanochemistry approaches, physicochemical treatment techniques are widely used for wastewater cleaning[33].

Some important methods that use nanomaterials are, for instance, adsorption and advanced oxidation processes (e.g. photocatalysis, Fenton processes, etc.)[33]. Besides oxidation processes and membranes, the adsorption method is considered a promising treatment process to remove and recycle the micropollutants from the water[30]. The adsorption technology is a competitive method for wastewater treatment[34]. Adsorption method is a surface phenomenon that is used in order to remove inorganic and organic pollutants[34]. Also, the adsorption technique by solid adsorbents represents a great potential to remove micropollutants in waste water treatment[34]. The adsorption process offers cost-effective pollution control due to its simple design[34,35].

Here we will mainly focus on adsorption since this is the main topic of this thesis.

1.3 Adsorption for wastewater treatment

The most general definition of adsorption is a phase transfer operation which is used to remove materials from liquid phase[30]. Adsorption is an effective removal method in water treatment[30].

The fundamental principle of adsorption theory is shown in Figure 4. The solid material (more precisely its surface) is called adsorbent; the species that are adsorbed on the surface of the

solid material are referred to as adsorbate[30]. The adsorbed materials can be released from the surface of the adsorbent by changing the characteristics of the fluid phases (e.g. temperature, concentration, and pH). The reverse system is named desorption[30].

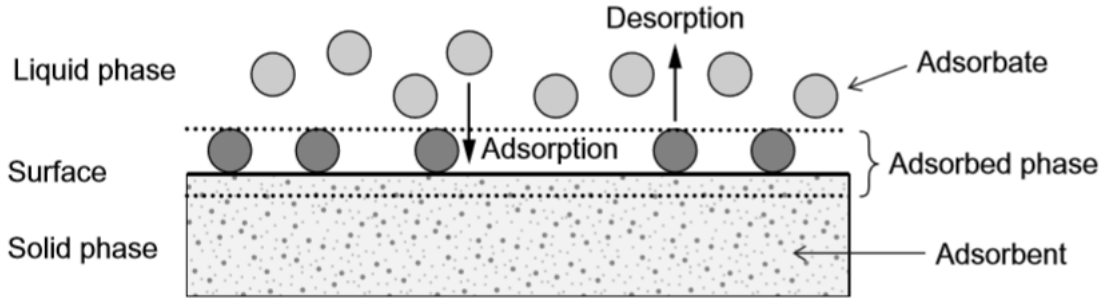

Figure 4: Fundamental terms of adsorption process[30]

There are generally two types of adsorbents: 1) natural adsorbents such as minerals, oxides, natural zeolites, clay or biopolymers; 2) engineered adsorbents such as carbonaceous adsorbents, zeolite molecular sieves and oxides[30].

Table 1 shows an overview of the most used applications, objectives and treatments. The most widely used adsorbent in wastewater cleaning is activated carbon which is produced from carbonaceous materials[30].

Table 1: Some application fields and used adsorbents in wastewater treatment[30]

Application field	Objective	Adsorbent
Drinking water	Removal of arsenic, organic materials and micro pollutants	Activated carbon, Iron hydroxide, Aluminum oxide
Industrial wastewater	Removal of specific chemicals	adsorbents, activated carbon
Urban wastewater	Removal of phosphate	Aluminium oxide, Iron hydroxide

As discussed in Section 1.1, azo dyes are the most used dyes in the textile industry, and they can have several toxic effects. Various nanomaterials were developed in order to remove from the water azo dyes and other toxic substances such as heavy metals and to protect the environment

and human health. Zeolites and oxides have a strong hydrophilic surface which shows good adsorption properties of charged species[15]. In particular, adsorption methods with oxides adsorbents (e.g. aluminium oxide, iron oxide and ferric hydroxide) are quite efficient in order to remove arsenate and selenium species[30]. Recently, engineered nanoparticles that have a size between 1 to 100 nanometers are used in many applications[36]. Also, engineered nanomaterials are promising for water treatment[30]. Thus, the use of engineered adsorbents is increasing for wastewater treatment due to being cost-effective materials and, having high adsorption capacities and large surface area[30].

Amongst these nanomaterials are carbon-based, metal oxide-based nanomaterials, hybrid (organic and inorganic) and polymer-based nanomaterials.

In recent decades, different kinds of carbon-based nanomaterials have been widely used to remove dyes and heavy metals due to their ease of preparation, porosity, high sorption capacity, abundance and nontoxicity[30]. Especially, activated carbon (AC), carbon nanotubes (CNTs) and graphene have been broadly used for removing dyes from wastewater[28].

AC is used mainly to remove organic solutes, pesticides, corrosion inhibitors, phenols and pharmaceuticals from groundwater, wastewater, aquarium water, swimming-pool water[30]. However, all raw waters have natural organic matter or pollutants that cannot be completely removed from water by using activated carbon. For instance, dye or heavy metal removal at ppb levels is difficult[30,37]. Also, activated carbon is not too selective when used for adsorption of organic substances[30].

Since CNTs discovery in 1991 by Iijima, CNTs have become useful nanomaterials in nanoscience, mainly owing to their considerable thermal, electronic, and mechanical properties[38,39]. Due to their unique adsorption capacity and properties, CNTs can be used in many applications[40,41]. CNTs can also be functionalized with other materials to extend their adsorption capacity[37]. Some studies show that multi-walled carbon nanotubes (MWCNTs) are more efficient than CNTs in the removal of dyes from aqueous solutions[37]. However, the disadvantage of CNTs is the high cost involved in the production[37].

Graphene has excellent mechanical, electrical and thermal properties, and unique 2D structure[37]. However, several studies show that graphene and functionalized graphene have a lower adsorption capacity than AC and CNTs[37].

Metal oxide-based nanomaterials are inorganic materials broadly used for removing dyes and heavy metal ions[37]. Especially, nanosized metal oxides such as TiO_2, Fe_3O_4, MnO_2, CdO, ZnO and

MgO have a high surface area[37,42]. So, these materials can be used for water treatment applications (adsorption, photocatalysis, coagulation, ultrafiltration, chemical precipitation and ion exchange)[42,43].

Also, metal oxide nanoparticles have low solubility and cause less secondary pollution formation than other materials[37]. Amongst all oxide-based materials, iron-based materials are promising and interesting for water treatment due to their magnetic properties[44,45]. Magnetism is an excellent physical feature that helps in water treatment[28,44]. Indeed the magnetic properties allow removing the materials easily from the water after their use for water purification[44,46]. Figure 5 shows a model of magnetic separation[47].

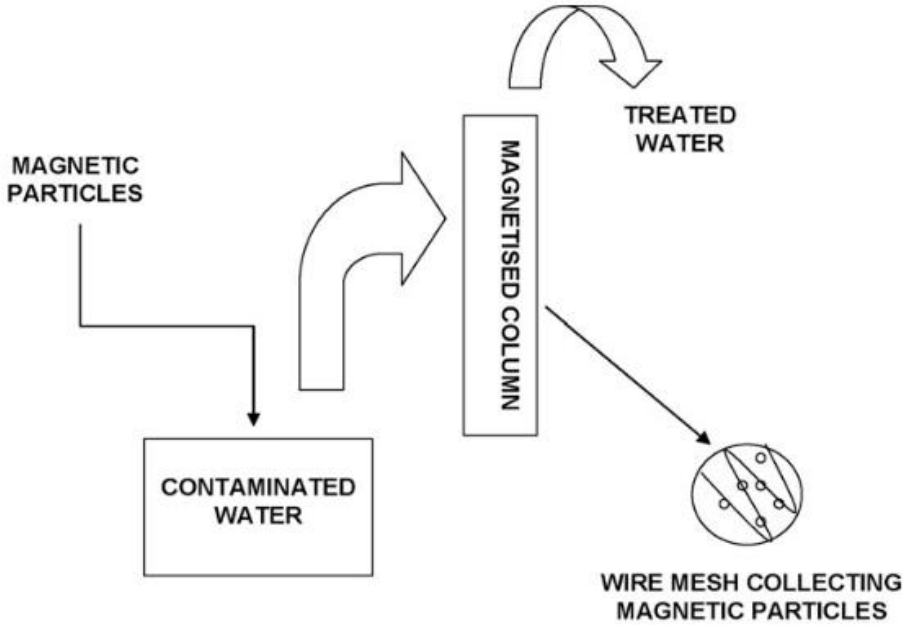

Figure 5: A schematic representation of magnetic separation[47]

As known, iron is one of the most common and eco-friendly element all over the earth[37]. Its abundance and the easy synthesis of iron oxides make them cost-effective for heavy metal ions and other molecules adsorption[37]. Many studies were reported in the literature regarding the removal of heavy metal ions by using Fe_3O_4 nanoparticles[37]. Further studies have reported about functionalized Fe_3O_4 by carboxyl-, amine- and thiol- groups for removing toxic metal ions from water[37,48,49]. Magnetic nanoparticles are highly efficient, economical, reusable and viable for removing the toxic metal ions from water[37]. Also, ferric nanoparticles have been applied to removing dyes (Reactive blue 19, reactive red 198, Neutral Red, Methylene Blue)[37].

1.4 Adsorption of dyes with microspheres

Polymeric adsorbents are obtained by copolymerization of weakly polar or nonpolar monomers, and they have higher adsorption characteristics than activated carbon, but higher costs[30,50,51].

Polymer-based nanomaterials help to achieve an effective removal of pollutants[52]. Polymeric adsorbents are environmentally harmless, possess excellent skeleton strength and easily modifiable surface groups, are relatively easy to functionalize[53]. Although polymer nanocomposites have great features, they show low adsorption capacity in aqueous solution. However, hybrid polymer/inorganic nanomaterials possess an improved adsorption capacity, and they might present other interesting properties[53].

In particular, microspheres are appropriate adsorbents for water cleaning because of their high loading capacity[54]. In this study, a hybrid nanocomposite based on magnetic microspheres was used (Figure 6). The magnetite Fe_3O_4 NPs/P(NIPAM-*co*-MAA) microspheres used in this thesis are made of a co-polymer of NIPAM (poly(N-isopropylacrylamide-*co* methacrylic acid) and methacrylic acid (MAA)[54]. After polymerization of NIPAM and MAA, the microspheres are doped with Fe_3O_4 magnetic nanoparticles[54]. The advantages of these microspheres in water cleaning are: 1) they adsorb dyes via the electrostatic interaction of chemical functional groups (carboxylic groups) on the surface of the microspheres with the pollutant[55]; 2) their adsorption capacity can be regulated intelligently due to the temperature, pH and magnetic responsive polymer segments. Also, the presence of the Fe_3O_4 magnetic nanoparticles allows the recyclability, after adsorption of the pollutant on the surface of the microspheres by applying an external magnetic field. The average diameter of the used microspheres is about 500 nm[54]. The microspheres bear several carboxylic groups on the surface that can attract other molecules electrostatically or via intermolecular interactions[54]. Thus, this property of the microspheres plays a significant role in the adsorption process[54]. Additionally, the surface of the microspheres can be easily modified with different groups such as chitosan, Fe_2O_3-SiO_2, Au@silica and $NaYF_4$-silica in order to enhance the adsorption capacity and efficiency[54,56,57].

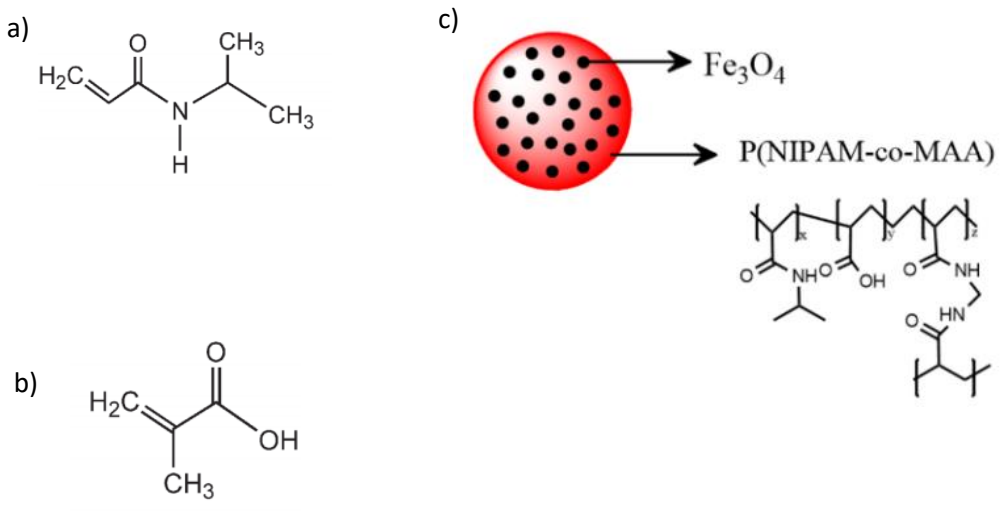

Figure 6: Schematic structure of a) *N*-isopropylacrylamide(NIPAM)[58], b) Methacrylic acid (MAA)[58] and c) Fe_3O_4/P(NIPAM-*co*-MAA) microspheres

In this thesis, the magnetic microspheres will be modified with PAMAM dendrimers in order to achieve a final nanocomposite able to adsorb different types of pollutants.

1.5 PAMAM dendrimers and their applications in waste water treatment

Dendrimers are radially symmetric, nano-sized, monodisperse, homogenous and highly branched polymeric nanoparticles[59]. Generally, dendrimers are divided into three parts: a core, branched units and surface groups[59]. Dendrimers are an interesting class of synthetic molecules and used in several applications due to their surface functionalization, high stability, hydrophilicity, tunable size and structure, both chemical and mechanical[60]. This class of hyperbranched polymers can be synthesized by two main approaches: divergent and convergent[61]. In divergent method, the synthesis of the dendrimers start from the core of the dendrimer to the arms of the dendrimer[62]. The arms are bind by adding building blocks step by step. In the convergent technique, the synthesis of the dendrimers begins from the exterior[59].

Dendrimers are mostly used in biomedical applications such as drug delivery, gene delivery, targeting component, imaging agents or detecting agents[63,64]. In environmental applications, dendrimers have been still scarcely used, but they show great potential in this field[65]. Dendritic nanopolymers, for instance, possess physicochemical properties which make them interesting as reaction and separation media for water treatment[66,67]. Dendritic nanopolymers contain dendrigraft polymers, hyperbranched polymers, dendrimers, supramolecular assemblies such

as dendrimer-like star polymers and core-shell tecto(dendrimers)[68] and they can encapsulate different cationic and anionic solutes[68].

Polyamidoamine (PAMAM) dendrimer is a highly branched, symmetric and nano-sized molecule with a monodisperse and homogeneous structure having an ethylenediamine (EDA) core and cationic outer surfaces (amino groups -NH_3^+)[60,61,69–71]. PAMAM dendrimers has an excellent relevance both scientifically and industrially[60]. PAMAM dendrimers are used in many applications, especially in biomedicine, drug delivery, gene delivery and host-guest chemistry[63,72]. PAMAM has unique properties such as high geometric symmetry, controllable internal voids, external functional groups, controllable size, structure and shape[72]. PAMAM dendrimers can be synthetized in different generations (From 0 to 11th generation)[60]. Different generations are used in different applications because of the number of branching points, the number of atoms and the number of nitrogen groups. In this study, 3rd, 4th and 5th generation of PAMAM dendrimer were used. 3rd (PAMAM G3), 4th (PAMAM G4) and 5th (PAMAM G5) generations of PAMAM dendrimer has respectively 1092, 2244 and 4548 total atoms and 32, 64 and 128 terminal nitrogen atoms[60]. Figure 7 shows the chemical structure of the PAMAM dendrimer. The generation of PAMAM dendrimer increases by an increase of branching points and therefore of final amino groups. In this thesis, a simplified structure of PAMAM dendrimer will be used in order to explain the reaction scheme (Figure 8).

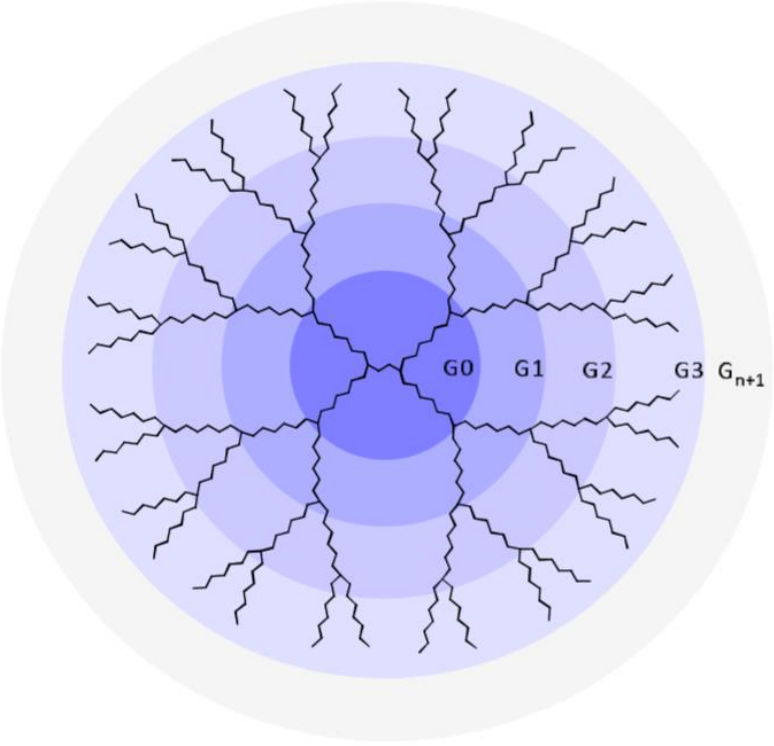

Figure 7: Schematic structure of PAMAM dendrimer[73]

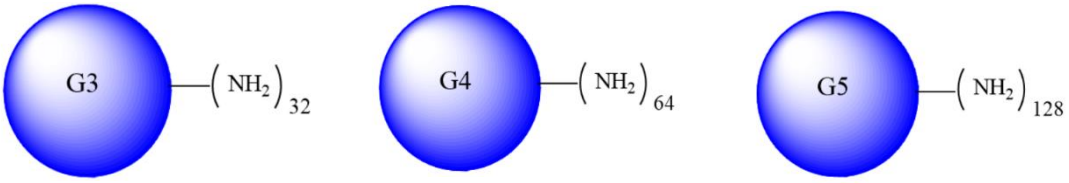

Figure 8: Simplified structure of PAMAM (G3), PAMAM (G4) and PAMAM (G5) dendrimer

Although PAMAM dendrimers have been extensively used in bio-application, there are still very few applications in the environmental field[72]. The dendrimer enhanced filtration process is one of the water treatment method [68]. In this process, there are three steps: 1) treatment; 2) dendrimer recovery; 3) and clean water recovery. As presented in Figure 9, polluted water is mixed with a solution that has functionalized dendritic nanopolymers to perform specific reactions of interest (e.g. anion and cation binding). Following, nanopolymer complexes with bonded contaminants are transferred to the recovery unit of clean water where the complexes are filtered by using ultrafiltration (UF) and microfiltration (MF) systems. In these systems, the bonded target substance is separated from nanopolymers by changing different parameters, for instance, pH[68]. Lastly, the nanopolymers are recycled by reintroducing the recovered materials on the treatment unit[68].

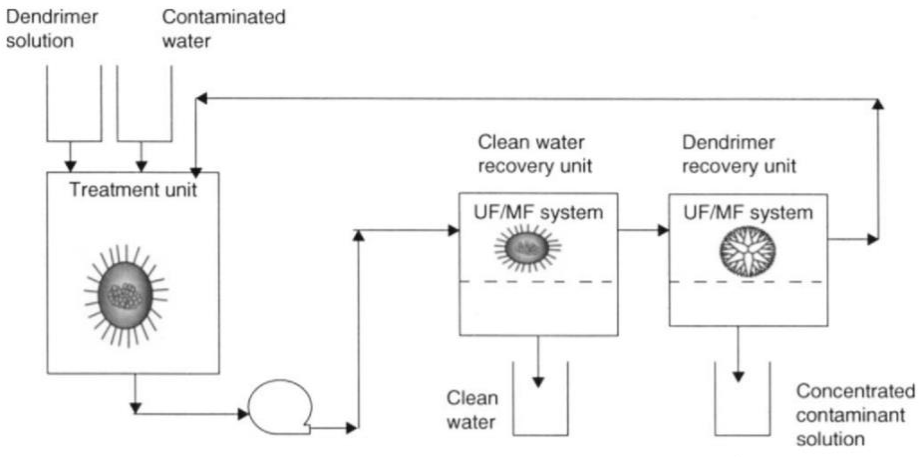

Figure 9: Water treatment by dendrimer enhanced filtration process[68]

Besides the filtration process, different studies regarding PAMAM dendrimers, different parameters (pH, temperature) and PAMAM with different surface groups are reported in the literature[74,75]. Modified PAMAM dendrimers with different terminal groups, such as graphene

oxide (GO), graphene sheet (GS), NH_2, COO^- and OH, is increasing in environmental studies[74]. One study shows the 3rd generation of PAMAM dendrimer grafted with different groups, such as GS, GO, OH and COO^- groups, to perform adsorption of heavy metal ions, such as Pb^{2+}, from aqueous solution[74]. The different modified PAMAM were compared to pure GS and GO. Figure 10 shows the Langmuir adsorption isotherm in which the variation of the total amount of Pb^{2+} ion adsorbed (q_e) onto different materials' surfaces is reported versus the ion concentration in water[74]. When the material used contains PAMAM, the adsorption of Pb^{2+} ions gives better results. From further calculations, it was determined that GO-PAMAM is the material able to adsorb the highest quantity of Pb^{2+} ions[74].

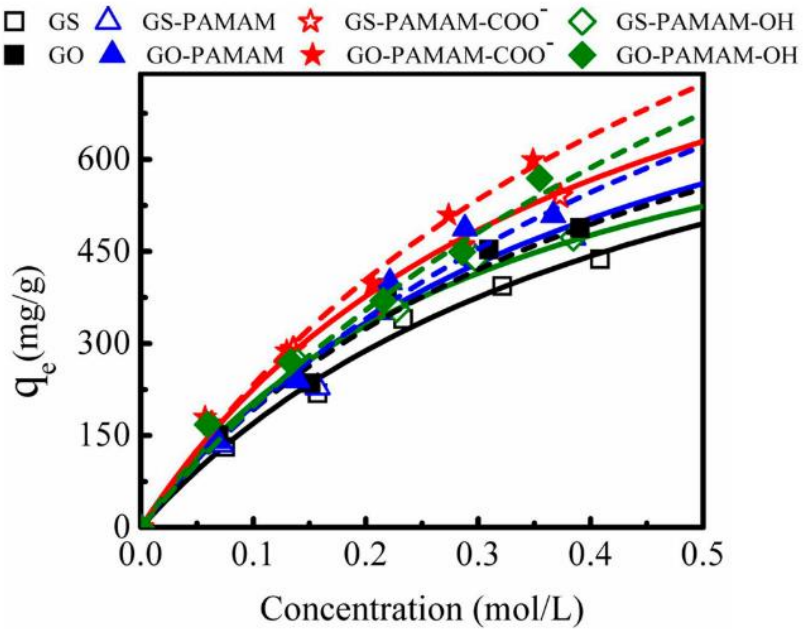

Figure 10: Variation of the total amount of adsorbed Pb^{2+} ions onto different surfaces versus ions concentration in water[74]

Another study about the removal of reactive blue 19 (RB19) dye using PAMAM (G3) and poly (propylene imine) dendrimers (PPI-G3) in wastewater is reported in the literature[75]. Especially, reactive anionic dyes are water-soluble and widely used in the textile industry, after azo dyes[66,75]. RB19 dye is very used in industries, has an anthraquinone chemical structure and therefore is highly photochemically stable and lasting in natural environments[75]. Thus, it causes environmental problems. In the study, the two different dendrimers were compared for the adsorption of RB19 by changing different parameters such as pH, dye concentration and adsorbent dosage. According to the results of this study, both dendrimers could adsorb efficiently the RB19[75]. Figure 11 shows the effect of different dye concentrations on RB19

removal efficiency by PAMAM (G3) in different pH values. As can be seen in the Figure, third generation PAMAM dendrimer can be used at different pH (at its best at low pH) and at different dye concentrations (also relatively high concentrations) as an eco-friendly adsorbent[75].

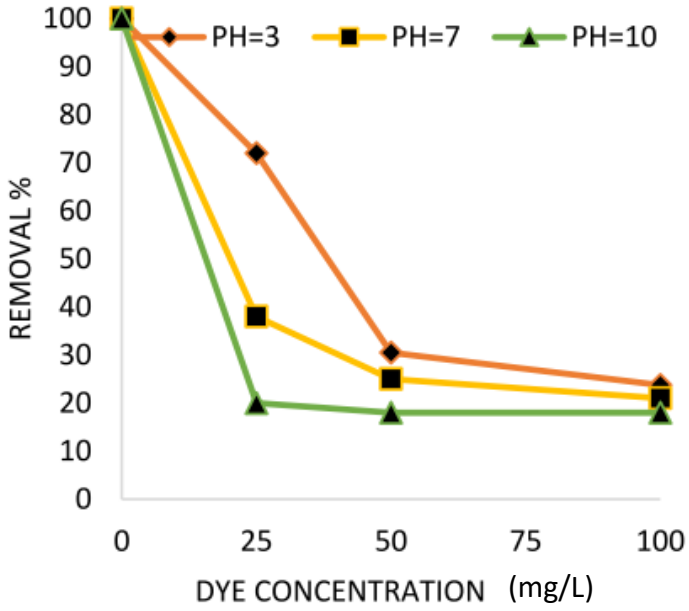

Figure 11: Removal efficiency by PAMAM (G3) in different pH values and at different initial dye concentrations[75]

The aim of this study is to combine Fe_3O_4/P(NIPAM-*co*-MAA) microspheres with PAMAM dendrimers (Generation 3, 4 and 5). The obtained nanocomposites will be tested for the adsorption of negatively and positively charged dyes.

1.6 Objectives

As it was discussed in the introduction, water is a very important source for all living organisms. However, pollutants are threatening freshwater sources. Water pollution is increasing due to the developing industry. Pollutants such as heavy metal ions and dyes, which come especially from the textile industry, are very toxic for environmental and human health. Dyes are the most common pollutants. In particular, azo dyes are highly toxic, have a complex structure and are particularly hard to degrade because they contain nitrogen-nitrogen double bonds (-N=N-)[10]. Also, in wastewater differently charged dyes might, often, be present. Removing these pollutants with a single method or material is hard by using traditional treatment techniques.

Physicochemical treatment techniques are a promising method for removing micropollutants from water. Amongst them, adsorption is very interesting because it gives the possibility to remove also molecules that are very difficult to degrade. The adsorbent can also be based on nanomaterials and, in this case, it has specific surface characteristics and higher surface area. In wastewater treatment processes, these properties provide the benefits of selectivity, increased affinity and capacity for the pollutants. Several are the materials used for adsorption. One of the most used is activated carbon (AC) due to its high adsorption capability[76]. Although AC is a promising adsorbent for wastewater treatment, it is not capable of removing the pollutants completely. More recently, magnetic thermo- and pH-responsive polymeric microspheres, namely Fe_3O_4/P(NIPAM-*co*-MAA), have been already used to remove dyes by adsorption. These microspheres are made of a co-polymer of NIPAM (poly(*N* -isopropylacrylamide- co methacrylic acid) and methacrylic acid (MAA) and are doped with Fe_3O_4 magnetic nanoparticles[54]. Thanks to the presence of NIPAM, the polymeric microspheres are thermo- and pH-responsive[54]. The presence of magnetite Fe_3O_4 nanoparticles makes the microspheres magnetic. The advantage of this system is that it is cheap, biocompatible, and it can be recycled thanks to its magnetic properties. However, often, there is the limitation that the system can adsorb only specific charged dyes.

In this study, magnetite Fe_3O_4 NPs/P(NIPAM-*co*-MAA) microspheres and different generations of Polyamidoamine (PAMAM) dendrimers have been combined to overcome this issue. The prepared nanocomposite can remove differently charged dyes and can be recycled thanks to its magnetic properties. In particular, the PAMAM dendrimer-grafted Fe_3O_4/P(NIPAM-*co*-MAA) nanocomposite bears on the surface carboxylic groups, due to the MAA in the structure of the polymer, and amino groups, due to the PAMAM dendrimer. In this way, positively charged and negatively charged dyes can be adsorbed from water. Due to the magnetic properties of the polymeric microspheres, the new nanocomposites can be recycled by applying an external magnetic field. In addition, since both polymeric microspheres and PAMAM dendrimers are non-toxic materials, eco-friendly nanocomposites were produced.

In this study, the adsorption of the positively charged dye basic fuchsin (BF) and the negatively charged azo dye methyl orange (MO) by using the prepared nanocomposites will be explored. In particular, the different nanocomposites prepared with different generations of dendrimers or a different molar ratio of dendrimer/polymers have been tested for the adsorption of BF and MO. The final aim is to obtain a new cost-effective and biocompatible nanomaterial able to adsorb both positively and negatively charged dyes, including the very resistant azo-dye MO. In

addition, the final system contains magnetic nanoparticles and, therefore, in future can be recycled after adsorption.

The thesis will be structured as follows:

In Section 2, a description of the materials and methods used is provided. In particular, it is explained how the nanocomposites were prepared, characterized, and how the adsorption tests towards BF and MO were performed. This Section also contains a short explanation of the principles of the main techniques used.

Section 3 consists of the results and discussion. In particular, after a session about the nanocomposites characterization, the nanocomposites were tested towards the adsorption of BF and MO.

Finally, in Section 4 the main conclusions are presented.

Chapter 2

2. Materials and methods

This section will be divided in four parts: 1) the synthetic pathway to prepare the PAMAM dendrimer-grafted Fe_3O_4/P(NIPAM-*co*-MAA) nanocomposites; 2) the characterization techniques; 3) the adsorption experiments performed with the nanocomposites to adsorb the two dyes, basic fuchsin and methyl orange; 4) the working principles of the used instruments.

2.1 Preparation of the PAMAM dendrimer-grafted Fe_3O_4/P(NIPAM-*co*-MAA) nanocomposites

2.1.1 Materials

Fe_3O_4/P(NIPAM-*co*-MAA) microspheres were synthesized by Jiao Wang *et al.* at TU Dresden according to the procedure reported in a published work[54]. PAMAM dendrimers were purchased from Dendritech. Reagents; N,N'-Dicyclohexylcarbodiimide (DCC) and Dimethylformamide (DMF) were purchased from Sigma-Aldrich (Dresden, Germany). 4-Dimethylaminopyridine (DMAP) was purchased from Merck (Dresden, Germany). Water was purified by an Astacus membraPure system and was used in all experiments (0.055 μS/cm).

2.1.2 Synthetic route for the preparation of the nanocomposites

The production of the PAMAM dendrimer-grafted Fe_3O_4/P(NIPAM-*co*-MAA) nanocomposites was performed by modifying a reported method for the coupling between amino and carboxylic groups[77] (for the detailed reaction scheme see section 3.1.1). In particular, the carboxylic groups of the Fe_3O_4/P(NIPAM-*co*-MAA) microspheres were coupled to the amine groups of the PAMAM (G3), PAMAM(G4) and PAMAM(G5) dendrimer to form new amide bonds[78]. The general pathway was performed through the following steps. PAMAM dendrimer was dissolved in DMF by using a magnetic stirrer. Then, Fe_3O_4/P(NIPAM-*co*-MAA) microspheres and DMAP were added to the dissolved PAMAM solution[77]. In this way, DMAP partially activated carboxylic groups of Fe_3O_4/P(NIPAM-*co*-MAA). After that, DCC was dissolved by using DMF in 15-mL flask. The dissolved DCC was added dropwise to the main solution to continue the activation of carboxylic groups of Fe_3O_4/P(NIPAM-*co*-MAA) and start the reaction. To keep the speed of the reaction low and avoid polymerization, the temperature was kept at 0 °C. Firstly, the solution was stirred for 2 hours at 0 °C and then, for 6 hours at room temperature. After the synthesis, the sample was

dialyzed (MWCO: 20 kD, Biotech RC Tubing) against dH_2O for 3 days. Freeze dryer (Christ-Alpha 1-4) was used in order to dry the samples.

Table 2 describes the used amounts of dendrimer, microspheres, DMAP, DCC and DMF, the calculated molar ratio between dendrimer's amino groups and polymer's carboxylic groups for each reaction performed and the different samples' name.

Table 2: The amounts of used chemicals, molar ratio between dendrimer's amino groups and polymer's carboxylic groups for each reaction and the different samples' name (DMF was used as solvent; 0.009 g of DMAP were used for all the syntheses of nanocomposites except for the synthesis of $G3_1P_1$ where 0.018 g of DMAP were used)

Sample´s name	PAMAM generations	Molar ratio of amino to carboxylic groups	PAMAM (g)	Fe_3O_4/P(NIPAM-*co*-MAA) (g)	DCC (g)
$G3_1P_1$	G3	1:1	0.016	0.048	0.03914
$G4_1P_1$	G4	1:1	0.008	0.024	0.01957
$G5_1P_1$	G5	1:1	0.008	0.024	0.01957
$G5_1P_{05}$	G5	1:0.5	0.016	0.024	0.03914
$G5_1P_{08}$	G5	1:0.8	0.016	0.038	0.03914

$G3_1P_1$, $G4_1P_1$ and $G5_1P_1$ nanocomposites were synthesized by using the molar ratio (1:1) of amino groups in the dendrimer to carboxylic groups in the microspheres. The reactions which have the molar ratio (1:1) of amino groups in the dendrimer to carboxylic groups in the microspheres were repeated; $G3_1P_1$ and $G4_1P_1$ were synthesised twice and $G5_1P_1$ three times. From the adsorption experiments, $G5_1P_1$ nanocomposite gave the best results when compared to the other two nanocomposites (for better details, see section 3.3.3). Therefore, a different molar ratio, which are (1:0.5 and 1:0.8) of amino groups and carboxylic groups were used to synthesize the new nanocomposites (see Table 2).

2.2 Characterization of the PAMAM dendrimer-grafted Fe_3O_4/P(NIPAM-*co*-MAA) nanocomposites

2.2.1 Instruments used

UV-Vis spectra were recorded with a Cary 100 Bio UV-Visible spectrophotometer. UV-Vis spectra were acquired in water using quartz cuvettes and water as a reference.

ATR-FTIR spectra were recorded with an IRaffinity-1S-ATR-FTIR from Shimadzu. The spectra were acquired by depositing the solid sample on the diamond crystal sample holder. The samples were measured by using the measurement mode transmittance (T%), number of runs 32 and resolution 2. After the spectra were obtained, the data are converted to ATR-FTIR data.

DLS spectra were recorded with a ZetaSizer Nano. The DLS spectra were acquired by using low-volume cuvettes in water and by 10 runs, 3 measurements, temperature 22°C, water as the solvent, angle 90°)

The samples were dried with Christ-Alpha 1-4 freeze dryer for 72 hours.

HR-TEM images were obtained using a 200 kV TEM microscope FEI Talos F200X, which combines high-resolution S/TEM with energy dispersive x-ray spectroscopy (EDS) signal detection, and 3D chemical characterization with compositional mapping. The specimen support used for TEM investigations was a microscopic copper grid covered by a thin transparent carbon film. A 3 ul of sample solution was dropped on grid and evaporated at room temperature. A 3 ul of phosphotungstic acid (5% suspension) was used for contrasting of the sample at grid.

2.3 Adsorption experiments procedure

2.3.1 Materials and methodologies

Basic fuchsin was purchased from Sigma-Aldrich and methyl orange (MO) from Merck.

For the adsorption experiments, the samples were collected in the dark at specific time points into 1.5 mL Eppendorf`s tubes and centrifuged for 10 minutes at 14000 rpm. The absorption spectra of the samples were recorded in water in quartz cuvettes by UV-Vis spectroscopy (Varian Cary 100 Bio UV-Vis spectrophotometer).

2.3.2 Experimental pathway for the adsorption experiments

The obtained nanocomposites $G3_1P_1$, $G4_1P_1$ and $G5_1P_1$ were tested to evaluate their adsorption ability against BF and MO in water. In order to perform the adsorption experiments, in advance, an aqueous solution of BF and MO was prepared at 0.015 mol/L concentration. All adsorption experiments were performed in the dark. Reference measurements were performed by using only the non-grafted Fe_3O_4/P(NIPAM-*co*-MAA) microspheres. Then, measurements were performed with each kind of composites, namely $G3_1P_1$, $G4_1P_1$ and $G5_1P_1$. For the

nanocomposites containing the PAMAM (G5), also the different nanocomposites prepared with different ratios of amino to carboxylic groups were tested for adsorption. For each experiment, 4 mg of the nanocomposite were added to 10 ml of an aqueous solution of BF and MO. While the aqueous solution was stirring (500 rpm) in the dark for 160 minutes, at different time points (5, 10, 20, 30, 40, 60, 80, 100, 130 and 160 min), 1 ml of solution was taken and centrifuged for 10 minutes (14000 rpm) to separate the nanocomposites from the dyes. Then, the supernatants were measured by UV-Vis spectroscopy to evaluate the discoloration of the solution during the adsorption experiment.

The kinetic adsorption experiments were performed in order to determine the adsorption rate of BF and MO by synthesized nanocomposites. The experimental data were analysed and evaluated by employing the Lagergren pseudo-first-order [1] and pseudo-second-order [2] models[54,79]. The kinetic constants and curves will be discussed in section 3.3.3.

$$\ln(q_e - q_t) = \ln q_e - k_1 t \qquad [1]$$

$$\frac{t}{q_t} = \frac{1}{k_2 {q_e}^2} + \frac{t}{q_e} \qquad [2]$$

In the given formula, q_e and q_t are the adsorption capacities (mg g^{-1}) of the nanocomposites at the adsorption equilibrium and at the time t (min), the adsorption rate constants are k_1 (min^{-1}) and k_2 (g mg^{-1} min^{-1}).

2.4 Working Principles of the instruments used

2.4.1 UV-Vis spectroscopy

Ultraviolet-Visible spectroscopy is a kind of absorption spectroscopy in ultraviolet and visible spectral regions[80]. It is used to measure the absorbance of the species in solution and can also be used for quantitative studies. For the UV-Vis technique, a light source and a spectrometer are needed. The energy range in which UV-Vis spectroscopy works is ultraviolet (200-400 nm) and visible (400-780 nm)[80].

A schematic representation of a dual beam UV-Vis spectrophotometer can be seen in Figure 12. The spectrophotometer is composed of a light source, a beam splitter, a sample and reference holders and a detector. Usually, in UV-Visible spectrophotometers, there are two light sources, one for the UV and one for the visible light emission. The beam is directed first to a filter[80] and then is split in two beams thanks to the beam splitter[80]. Monochromatic light crosses two

cuvettes, one of them has the reference solution (distilled water), the other cuvette is the sample which is used in the experiment (in the case of this study the solution are composed of BF or MO)[80]. The light that was not absorbed by the samples is collected and amplified thanks to a photomultiplier and the data are transferred to a computer. After that, the data are shown as a graph of absorbance versus wavelengths and the peaks represent the maximum absorbance[80]. For MO the maximum absorbance peak is at 463 nm; at 542 nm for BF.

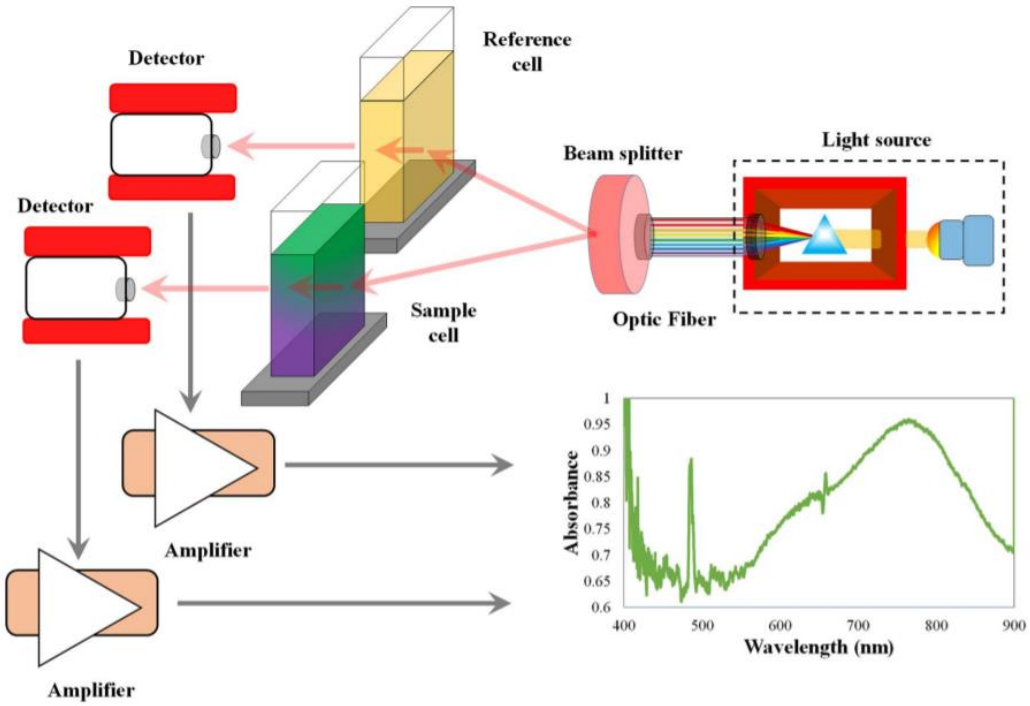

Figure 12: A schematic diagram of a UV-Visible setup[80]

The absorbance of the species in the sample is directly connected to the concentration of that species in the solution. The equation [1] which is named the Lambert-Beer Law is the mathematical-physical representation of light-absorption measurements[80,81]. The absorbance (Abs) is measured as described below:

$$log\frac{I_0}{I} = \varepsilon(\lambda).x.c = Abs(\lambda) \qquad [1]$$

where I_0 is the intensity of the incident light and I is the intensity of the transmitted light; x is the path length of the cuvette, c is the molar concentration of the absorbing molecule, $\varepsilon(\lambda)$ is the extinction coefficient and Abs is the absorbance at the wavelength(λ)[80]. This law shows that inside the limits of its validity, the concentration of the absorbing species is proportional to its absorbance.

2.4.2 FTIR (Fourier Transform Infrared) spectroscopy

Fourier transform-Infrared (FT-IR) spectroscopy is used in order to identify the structures of the samples and the kind of molecular bonds in the molecules[80,82]. Figure 13 shows the schematic of an FT-IR setup. As the primary excitation source, infrared radiation (IR) is used in FT-IR spectroscopy[82]. The spectrum is obtained from the absorption of IR radiation by the sample[80]. With IR radiation, it is possible to excite the vibrational states of molecules. In this way, the IR absorption peaks in the spectra represent certain molecular bonds and make molecular identification possible[80]. The IR sensor records transmitted radiation intensity signals as a wavelength function in the form of an interferogram[80]. Computer algorithms play a role in order to convert the interferogram to an IR absorbance spectrum by using Fourier transformation[80]. A classical FTIR spectrum is represented/plotted by the intensity of transmitted IR spectra versus wavenumber (cm^{-1})[80,82]. The obtained peaks in the spectrum correspond to different molecular bonds and, therefore, different functional groups can be identified[80,82]. The Lambert-Beer Law equation is used to explain the linear relationship between absorbance (A) and concentration(c). In equation [2] absorbance is A, molar absorptivity is ε, and path length is b'[82].

$$A = \varepsilon . c . b' \qquad [2]$$

Some special kinds of FTIR spectrometers have a unit called Attenuated Total Reflectance (ATR)[83]. These spectrometers contain a sample holder made of a crystal (for this thesis it is a diamond crystal) able to reflect light several times. This amplifies the signal coming from functional groups placed at the surface of the samples. However, to compare the ATR-FTIR spectra to normal IR spectra, a correction for the light attenuation in the diamond crystal is needed. In this study, the data obtained are used to identify the molecular structure of the samples[82].

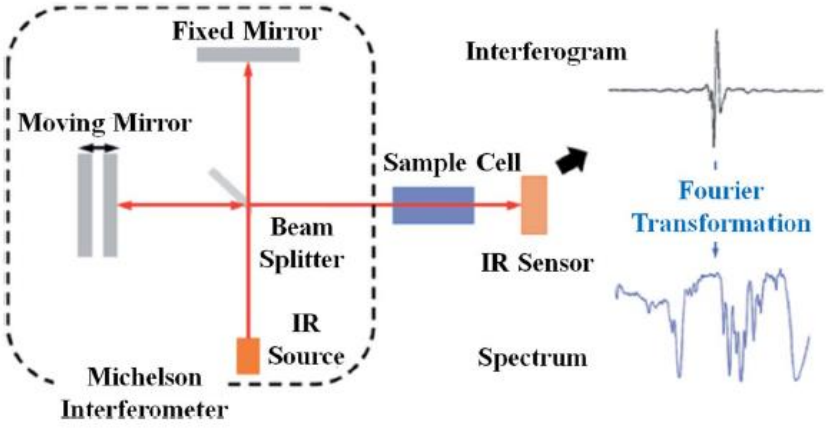

Figure 13: A schematic diagram of an FTIR setup[80]

2.4.3 DLS (Dynamic Light Scattering)

Dynamic Light Scattering (DLS) is a technique which is used to measure the size of particles and polymers in solution; in this study, Malvern ZetaSizer Nano ZS Series was used. The technique allows measuring the hydrodynamic size of the samples[84,85]. In a solution, all the particles move randomly in any direction. That random movement is called Brownian motion[84]. Smaller dimension particles move through much longer distances than bigger particles[84]. Also, bigger particles scatter more light than small dimension particles. The setup of the DLS is shown in Figure 14.

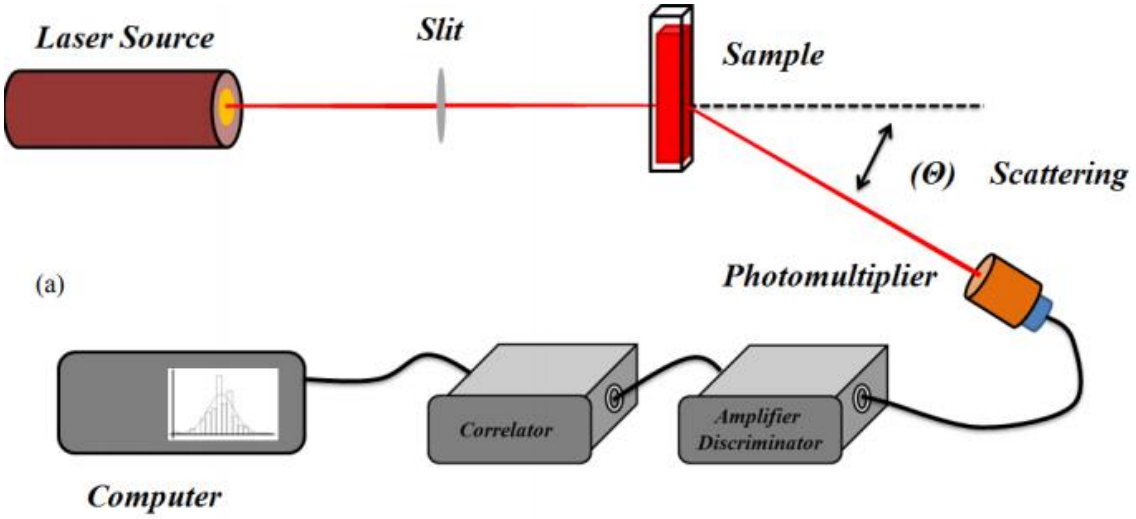

Figure 14: A schematic diagram of a DLS setup[86]

In order to calculate the hydrodynamic diameter of the particles, the Stokes-Einstein equation [3] is used[87]. d(H) is the hydrodynamic diameter, *k* is the Boltzmann Constant, T is the absolute temperature, η is the solvent viscosity, and D is translational diffusion coefficient[85].

$$d(H) = \frac{kT}{3\pi\,\eta\,D} \qquad [3]$$

The DLS graphs are number (%), intensity (%) and volume (%) distributions plotted versus size. The graph of number (%) versus size shows a number of nanoparticles with a certain size in the solution. The intensity (%) versus size gives information about the intensity of scattered light. The volume (%) versus size graphs can be obtained, converting the intensity (%) distribution graphs. The volume distribution graphs describe the components in the sample based on their volume.

2.4.4 HR-TEM (High-Resolution Transmission Electron Microscopy)

Transmission Electron Microscopy is a technique in which an electron beam is used in order to form an image of the sample[86]. This electron beam is emitted using a lanthanum hexaboride or tungsten filament[86,88]. Firstly, the electron beam passes through a condenser lens then, it passes through the specimen by an objective lens. The electron beam provides a higher resolution than the visible light in optical microscopy[88]. In general, high energy primary electrons pass through the specimen then, the electrons deflect from the samples in order to create an image in electron microscopy[86,88]. In TEM, the electron beams are transmitted through the ultrathin specimen then, it is transformed into a non-uniform electron intensity after scattering or transmission by the specimen[88]. An ultra-high vacuum which prevents electron scattering is used in order to analyse the sample in TEM[88]. So, electrons can move easily from the gun to the specimen and then to the detector[88]. Figure 15 shows the schematic diagram of a TEM microscope.

High-Resolution Transmission Electron Microscopy (HR-TEM) is a mode of imaging which uses both the scattered and transmitted beams in order to create interference image[89]. HR-TEM is a powerful technique to study features of materials on the atomic scale, for instance, nanoparticles, semiconductors and metals. HR-TEM is used in order to obtain high-resolution scanning TEM[89].

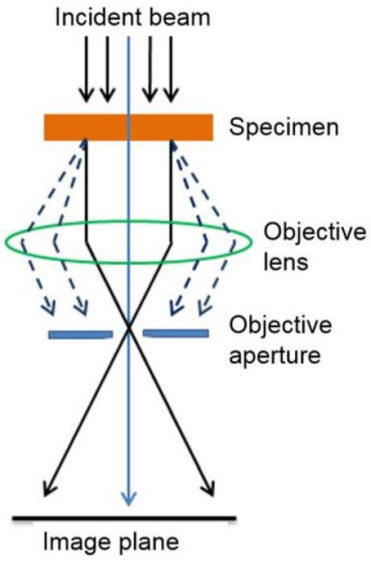

Figure 15: A schematic diagram of a TEM setup[88]

Chapter 3

3. Results and discussion

This Section will be divided into two main parts: 1) the preparation, calculations and characterization of the PAMAM dendrimer-grafted Fe_3O_4/P(NIPAM-*co*-MAA) nanocomposites; 2) the adsorption experiments to test the different samples for the adsorption of the two differently charged dyes, BF and MO.

3.1 Preparation and Characterization of the PAMAM dendrimer-grafted Fe_3O_4/P(NIPAM-*co*-MAA) nanocomposites

3.1.1 Synthesis of the nanocomposites

Several samples were prepared by combining the Fe_3O_4/P(NIPAM-*co*-MAA) microspheres with PAMAM dendrimers of different generations. The samples were prepared as described in detail in section 3.1.2. A schematic representation of the reaction is reported in Figure 16. In particular, the carboxylic groups of the Fe_3O_4/P(NIPAM-*co*-MAA) microspheres were coupled to the amino groups of the PAMAM (G3), PAMAM(G4) and PAMAM(G5) dendrimer to form amide bonds modifying a coupling reported method[77].

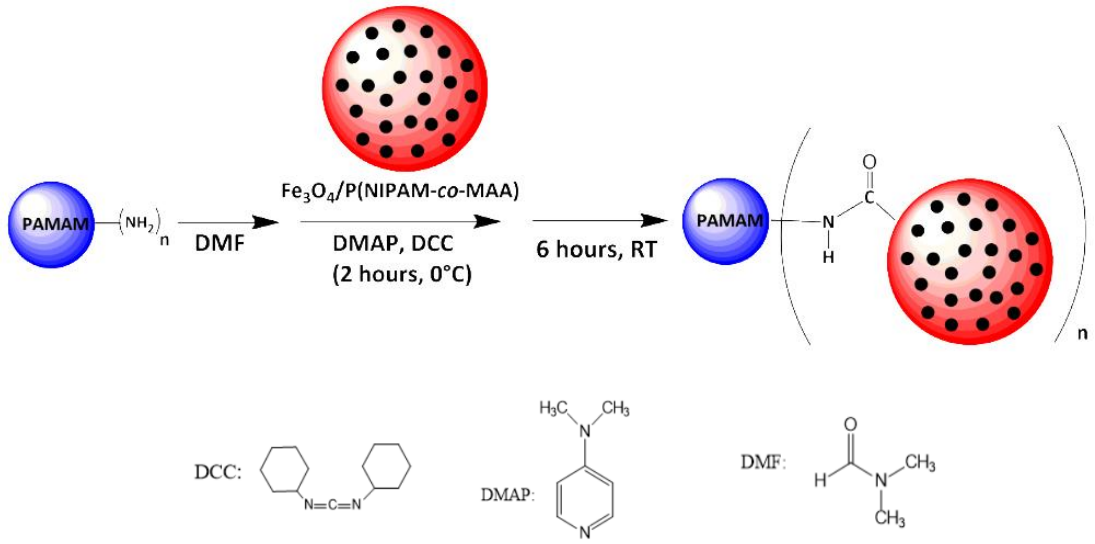

Figure 16: A schematic representation of the reaction of preparation of the PAMAM dendrimer-grafted magnetic Fe_3O_4/P(NIPAM-*co*-MAA) nanocomposites

Several reactions were performed by changing the dendrimer generation or by keeping the same generation but changing the ratio between the dendrimer and the polymer. The samples that will be studied in this thesis are reported in Table 3.

Table 3: Correspondence between sample´s name and the initial molar ratio between dendrimer´s amino and polymer´s carboxylic groups to prepare the nanocomposites

Sample´s name	PAMAM generations	Molar ratio of amino to carboxylic groups
$G3_1P_1$	G3	1:1
$G4_1P_1$	G4	1:1
$G5_1P_1$	G5	1:1
$G5_1P_{05}$	G5	1:0.5
$G5_1P_{08}$	G5	1:0.8

The samples were then characterized by different techniques (FTIR, DLS, UV-Vis and HR-TEM) and then used in the adsorption experiments.

3.1.2 ATR-FTIR spectra of the PAMAM dendrimer-grafted Fe_3O_4/P(NIPAM-*co*-MAA) nanocomposites

ATR- FTIR spectra of PAMAM (G3), PAMAM (G4), PAMAM (G5), Fe_3O_4/P(NIPAM-*co*-MAA) microspheres and the PAMAM dendrimer-grafted Fe_3O_4/P(NIPAM-*co*-MAA) nanocomposites were recorded, and the graphs were corrected by using ATR correction to be directly compared with conventional infrared spectra. Figure 17, 18 and 19 show the ATR-FTIR spectra (after ATR correction) of $G3_1P_1$, $G4_1P_1$, $G5_1P_1$ nanocomposites compared to the Fe_3O_4/P(NIPAM-*co*-MAA) microspheres and the PAMAM dendrimers. As can be seen in these Figures, all the new nanocomposites present the typical peaks of both the PAMAM dendrimer and the Fe_3O_4/P(NIPAM-*co*-MAA) microspheres meaning that the nanocomposites contain both components. Indeed, the spectra of PAMAM dendrimers show the following characteristic peaks, the N-H peaks at around 3280 cm^{-1} and 1556 cm^{-1}, the C=O peak at around 1645 cm^{-1} [78]. Also, the Fe_3O_4/P(NIPAM-*co*-MAA) microspheres have their own characteristic peaks which are the N-H peaks at around 3220 cm^{-1}, the C=O peaks at around 1620 cm^{-1} and the -CH_2 peaks at

around 1540 cm^{-1} (See Figure 17, 18 and 19)[54,64]. Nevertheless, it has to be noted that the ATR-FTIR spectra for the PAMAM dendrimer and the Fe_3O_4/P(NIPAM-*co*-MAA) microspheres show very similar peaks.

In the spectra of the nanocomposites, the peaks of the amide bonds formed between the polymeric microspheres and the PAMAM dendrimer are hard to see since they fall at 1650 cm^{-1} (C=O of amide) and at 1530 cm^{-1} (N-H of amide)[77]. This is a region where both the polymeric microspheres and the PAMAM dendrimer present several peaks, so it is hard to distinguish eventual new peaks.

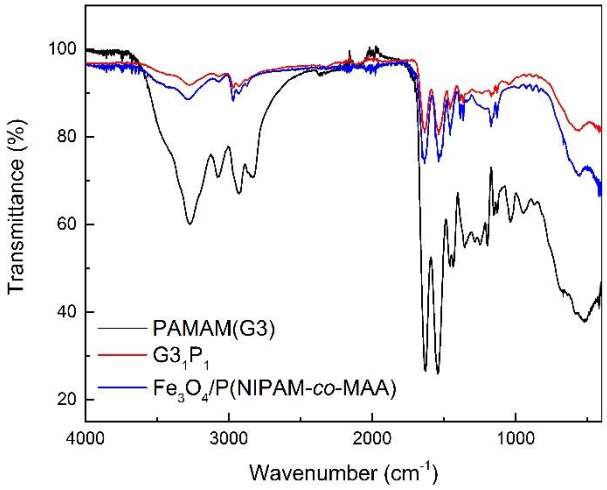

Figure 17: ATR- FTIR spectra of PAMAM (G3), Fe_3O_4/P(NIPAM-*co*-MAA) microspheres and $G3_1P_1$ nanocomposite

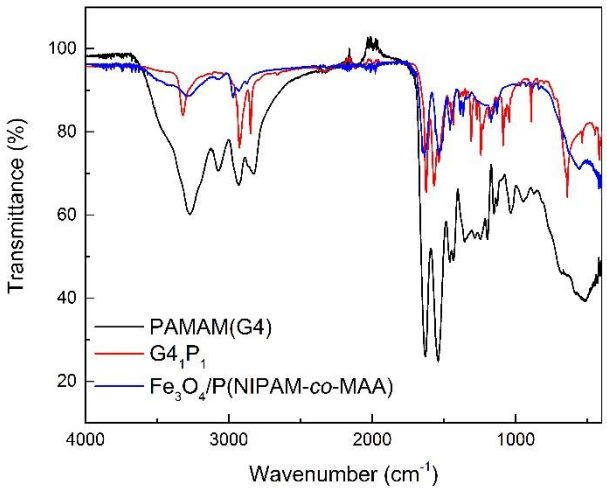

Figure 18: ATR- FTIR spectra of A) PAMAM (G4), Fe_3O_4/P(NIPAM-*co*-MAA) microspheres and $G4_1P_1$ nanocomposite

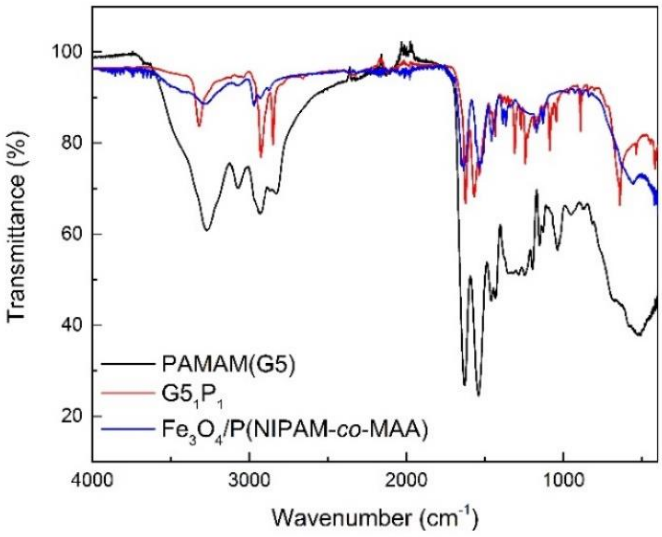

Figure 19: ATR- FTIR spectra of PAMAM (G5), Fe_3O_4/P(NIPAM-*co*-MAA) microspheres and $G5_1P_1$ nanocomposite

3.1.3 DLS spectra of the PAMAM dendrimer-grafted Fe_3O_4/P(NIPAM-*co*-MAA) nanocomposites

The polymeric microspheres and the nanocomposites were characterized by DLS to assess their hydrodynamic diameter. Each sample was prepared in 1 mg/ml concentration. As it can be seen in Figure 20, the hydrodynamic diameters of the polymeric microspheres is roughly 750 nm. A similar size of around 500-700 nm is found in the nanocomposites (See Figure 20). This is by the fact that dendrimers are only a few nanometers in size[90,91]. In addition, objects bigger than 1 µm are very close to the detection limit of the instrument and. Therefore, the presence of eventual bigger nanocomposites cannot be evaluated with these measurements.

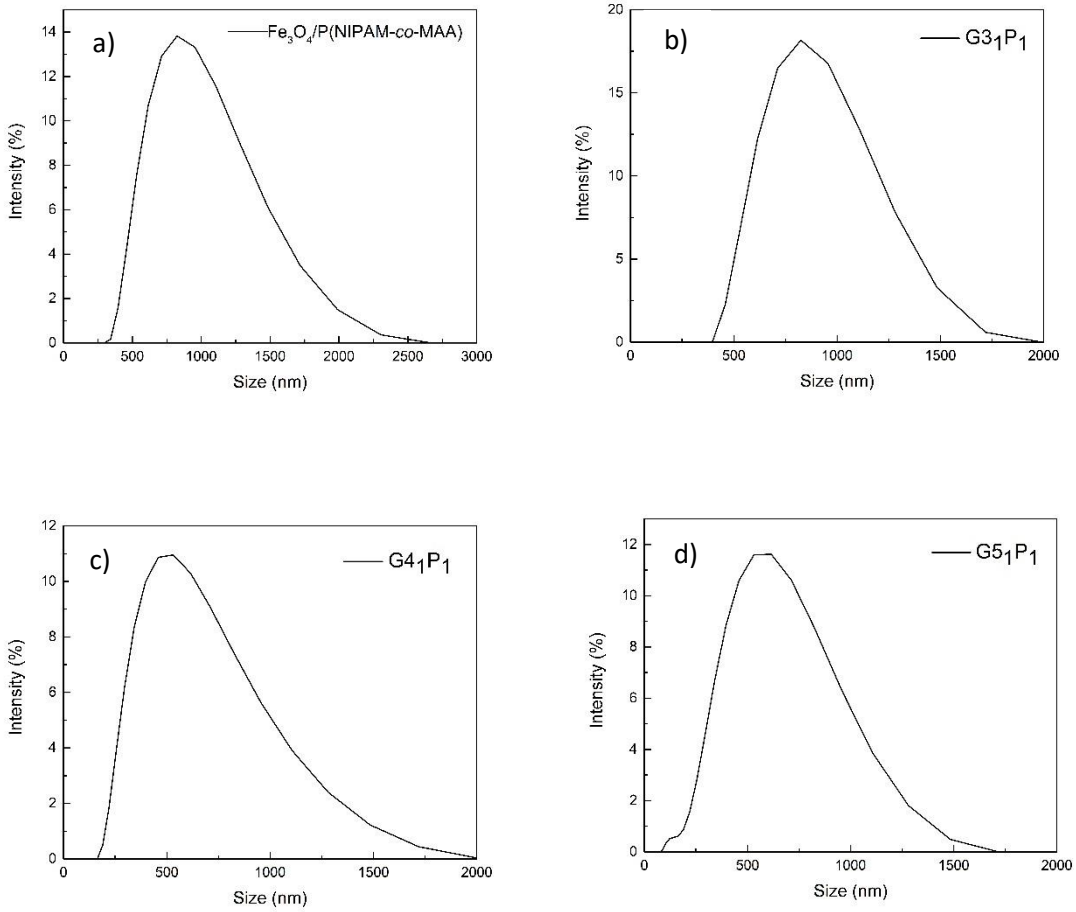

Figure 20: DLS of a) Fe_3O_4/P(NIPAM-*co*-MAA) microspheres, b) $G3_1P_1$, c) $G4_1P_1$ and d) $G5_1P_1$ nanocomposites

3.1.4 UV-Vis spectra of the PAMAM dendrimer, Fe_3O_4/P(NIPAM-*co*-MAA) microspheres and the PAMAM dendrimer-grafted Fe_3O_4/P(NIPAM-*co*-MAA) nanocomposites

To perform the UV-Vis measurements, samples were prepared in 0.05 mg/ml concentration. As it is shown in Figure 21, the PAMAM dendrimers, the Fe_3O_4/P(NIPAM-*co*-MAA) microspheres and the nanocomposites do not have any characteristic peak in the range of 200 nm-800 nm. However, they all absorb in the region below 250 nm for the dendrimers and below 400 nm for the polymer. The nanocomposites show absorbance in the same region.

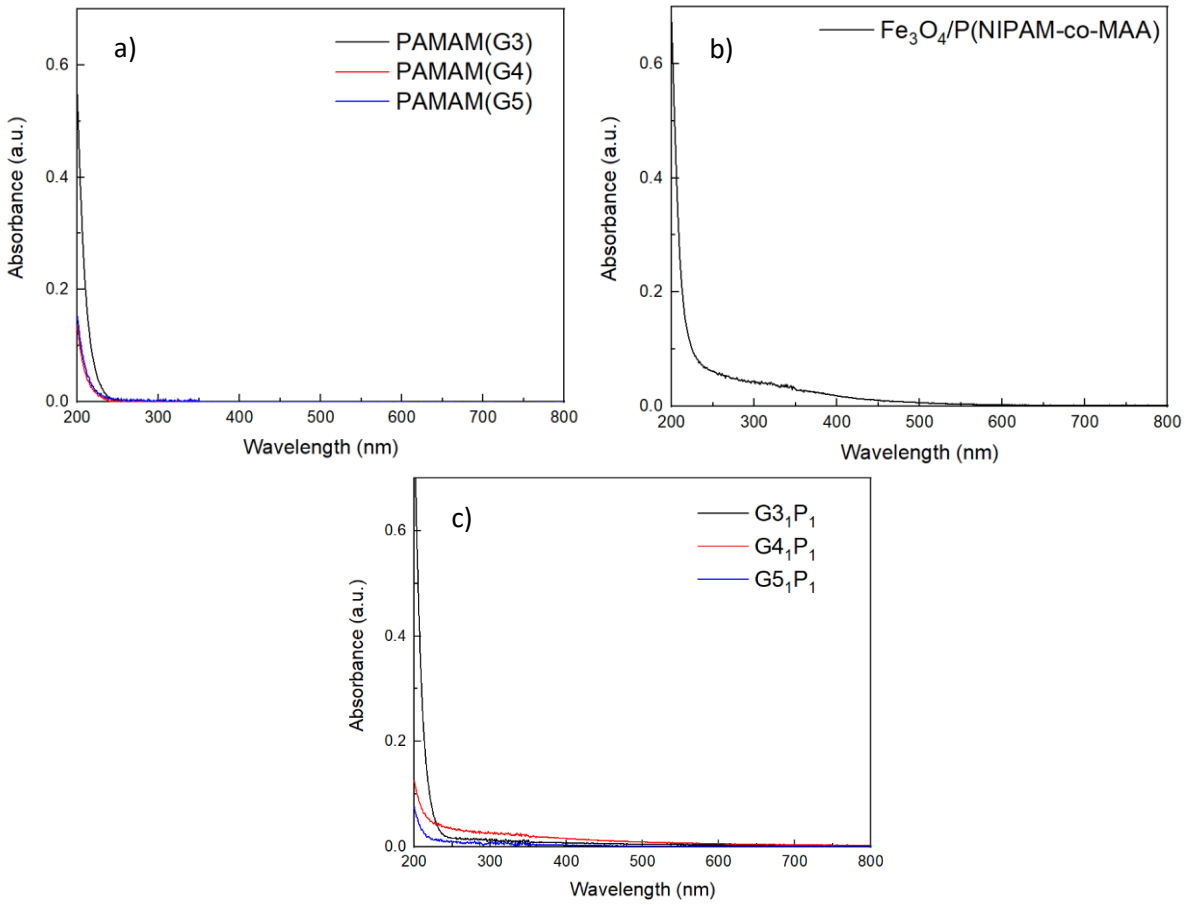

Figure 21: UV-Vis spectra of a) PAMAM dendrimers, b) Fe_3O_4/P(NIPAM-*co*-MAA) microspheres, c) $G3_1P_1$, $G4_1P_1$ and $G5_1P_1$ nanocomposites

3.1.5 HR-TEM images of the Fe_3O_4/P(NIPAM-*co*-MAA) microspheres and the PAMAM dendrimer-grafted Fe_3O_4/P(NIPAM-*co*-MAA) nanocomposites

HR-TEM was used in order to determine the size and shape of the PAMAM dendrimer-grafted Fe_3O_4/P(NIPAM-*co*-MAA) nanocomposites. Figure 22 a) shows that Fe_3O_4/P(NIPAM-*co*-MAA) microspheres have a size of around 400 and 500 nm, as reported in the literature. In Figure 23 a) the HR-TEM image of the nanocomposite $G4_1P_1$ is reported (images for the other nanocomposites were similar). After the coupling of the PAMAM dendrimers and Fe_3O_4/P(NIPAM-*co*-MAA) microspheres in the nanocomposite (Figure 23), the structure of the microspheres is retained and the size is similar to that of the Fe_3O_4/P(NIPAM-*co*-MAA) microspheres. In Figure 22 b) and 23 b), HAADF maps for the Fe_3O_4/P(NIPAM-*co*-MAA) microspheres and for the nanocomposite $G4_1P_1$ are reported. In particular, in Figure 22 b) only iron signal is mapped, while in Figure 23 b) both iron and oxygen signals are mapped. From these maps, it is possible to prove the presence of Fe_3O_4 nanoparticles both in the Fe_3O_4/P(NIPAM-*co*-

MAA) microspheres and in the $G4_1P_1$ nanocomposite. In addition, although it is difficult to visualize dendrimers in HR-TEM, bigger aggregates of dendrimers might be present around the microspheres in the nanocomposite $G4_1P_1$. Indeed, in Figure 23 b) it is evident that dendrimers aggregates, that do not contain oxygen, result colourless in the map.

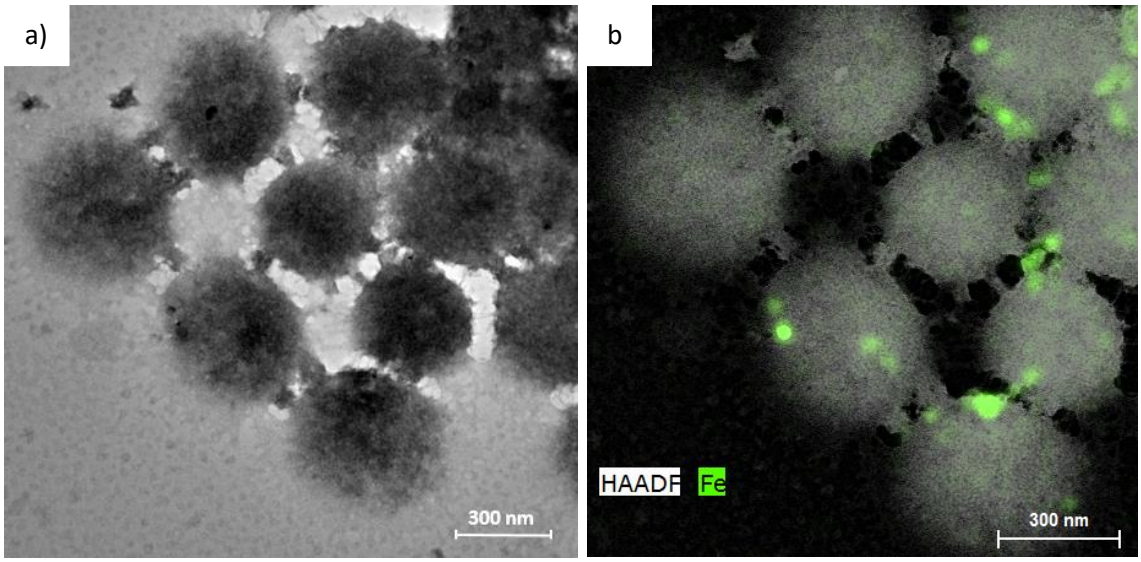

Figure 22: a) HR-TEM image for Fe_3O_4/P(NIPAM-*co*-MAA) microspheres, b) HR-TEM mapping image of Fe_3O_4/P(NIPAM-*co*-MAA) microspheres

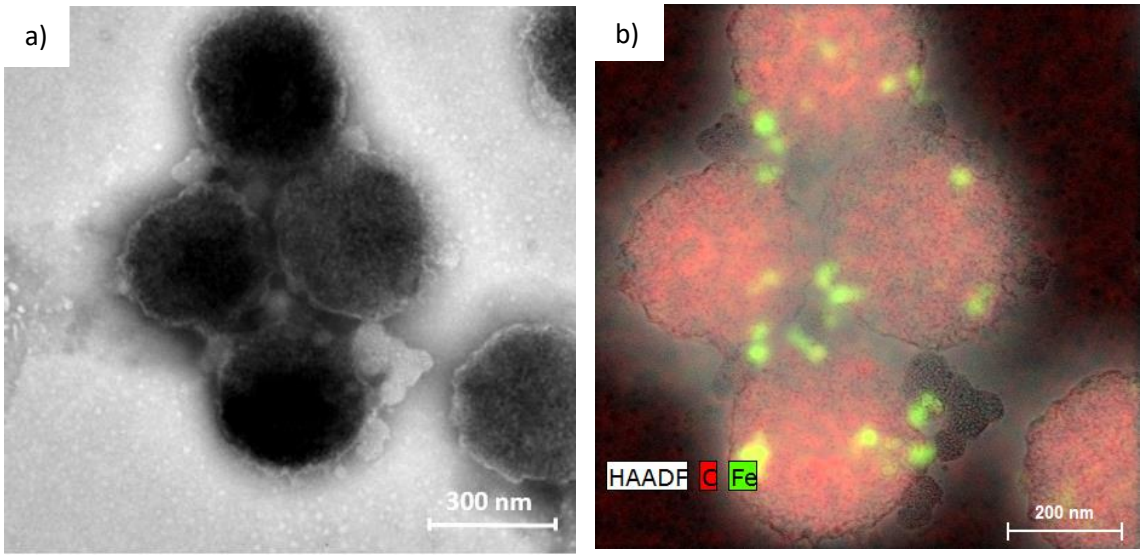

Figure 23: a) HR-TEM image for $G4_1P_1$, b) HR-TEM mapping image of $G4_1P_1$

3.2 Calculation of amino and carboxylic groups for the nanocomposite preparation

The calculations are reported in Appendix.

3.3 Application: Adsorption of dyes with the PAMAM dendrimer-grafted Fe_3O_4/P(NIPAM-*co*-MAA) nanocomposites

3.3.1 Adsorption of basic fuchsin

The adsorption ability of the obtained PAMAM dendrimer-grafted Fe_3O_4/P(NIPAM-*co*-MAA) nanocomposites were tested both with basic fuchsin, a cationic dye, and methyl orange, an anionic dye. The same experiments were performed with the Fe_3O_4/P(NIPAM-*co*-MAA) microspheres for comparison (For experimental details see Materials and Methods section). Figure 24 shows the absorption spectra for BF (initial concentration for all the experiments is 0.015 mol/L) in water at different times after adsorption on respectively Fe_3O_4/P(NIPAM-*co*-MAA) microspheres, $G3_1P_1$, $G4_1P_1$and $G5_1P_1$ nanocomposites.

As can be seen in Figure 24a, Fe_3O_4/P(NIPAM-*co*-MAA) microspheres adsorb BF in water quickly and effectively. Already 82.71% of BF is adsorbed after 20 minutes. However, after 20 minutes, there is a continuous adsorption/desorption of the dye from the surface.

In Figure 24b, the absorption spectra of BF at different times of adsorption on $G3_1P_1$ nanocomposite are presented. The absorbance of BF is decreasing with time, and after 30 minutes, 37.53% of BF is adsorbed. However, also in this case, for longer times here is a continuous adsorption/desorption process. Figure 24c shows the absorption spectra for BF in water at different times of adsorption with $G4_1P_1$ nanocomposite. $G4_1P_1$ does not adsorb the dye as quickly as the polymer alone, but it adsorbs the dye continuously till 160 minutes and much more effectively than $G3_1P_1$. The percentage of adsorption is 63.54% after 160 minutes and no adsorption/desorption is observed. In figure 24d, the graph shows the absorption spectra for BF in water at different times of adsorption with $G5_1P_1$ nanocomposite. The nanocomposite adsorbs BF efficiently and quickly. There is a continuous adsorption, and after 160 minutes, the adsorption of BF is 88.92%. This result is comparable with what obtained for the adsorption of BF with the polymeric microspheres. The kinetics of adsorption with the $G5_1P_1$ nanocomposite seems to be slower, but on the other hand the adsorption is continuous and no

adsorption/desorption is observed. According to these results, $G5_1P_1$ is the most promising nanocomposite.

To summarize, the nanocomposites show the following trend towards adsorption of BF:

$G5_1P_1 \geq Fe_3O_4$/P(NIPAM-*co*-MAA) microspheres > $G4_1P_1$ > $G3_1P_1$

This means that the presence of increasing generations of dendrimer increases the adsorption capability of the nanocomposite towards BF, reaching a comparable result to the polymeric microspheres in the absence of dendrimer.

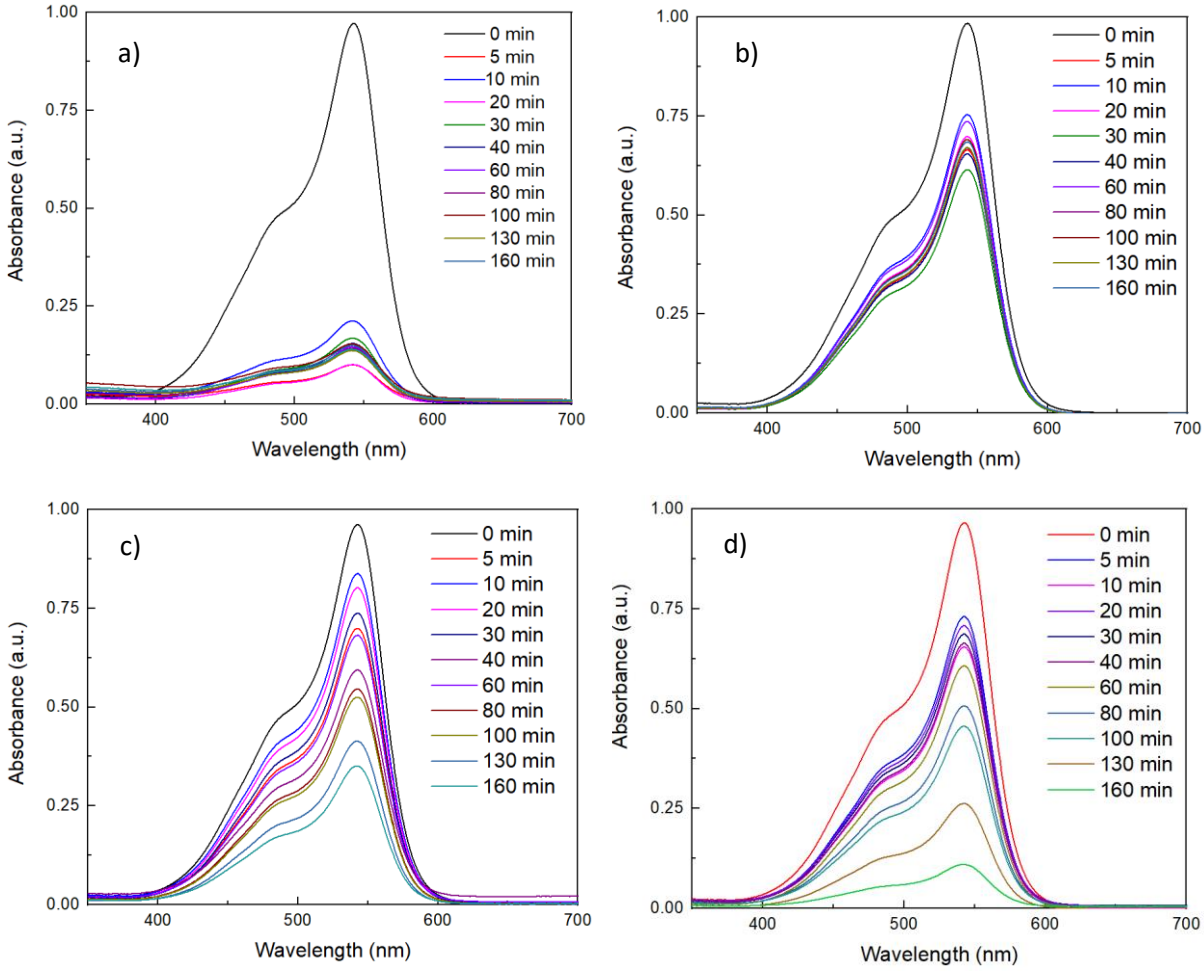

Figure 24: UV-Vis spectra of BF in the water at different times of the adsorption experiment with a) Fe_3O_4/P(NIPAM-*co*-MAA) microspheres, b) $G3_1P_1$, c) $G4_1P_1$ and d) $G5_1P_1$ nanocomposites

3.3.2 Adsorption of methyl orange

Figure 25 shows the absorption spectra for MO (initial concentration for all the experiments is 0.015 mol/L) in the water at different times after adsorption on respectively Fe_3O_4/P(NIPAM-*co*-MAA) microspheres, $G3_1P_1$, $G4_1P_1$ and $G5_1P_1$ nanocomposites. As can be seen in figure 25a, Fe_3O_4/P(NIPAM-*co*-MAA) microspheres do not adsorb MO. The percentage of adsorption is close to zero even after 160 minutes of adsorption. This is the reason why only spectra at t = 0 minutes and t = 160 minutes are shown. Figure 25b shows the absorption spectra of MO at different times of adsorption on $G3_1P_1$ nanocomposite. 9.73% of MO was adsorbed by $G3_1P_1$ after 20 minutes. After that, there is a continuous adsorption/desorption process. Figure 25c shows the absorption spectra for MO in water at different times of adsorption of MO with $G4_1P_1$ nanocomposite. $G4_1P_1$ shows similar behaviour to $G3_1P_1$ nanocomposite. The nanocomposite $G4_1P_1$ could only adsorb 8.49% of MO at 40 minutes. After that, there is again a continuous adsorption/desorption process. In figure 25d, the graph shows the absorption spectra for MO in water at different times of adsorption on $G5_1P_1$ nanocomposite. $G5_1P_1$ could adsorb MO continuously until 160 minutes and, after this time, 17.75% of MO was adsorbed. These results are very interesting because all nanocomposites adsorb more MO than the only polymeric microspheres that cannot adsorb MO. In particular, $G5_1P_1$ is very promising because the adsorption of MO is continuous and reaches 17.75% after 160 minutes.

To summarize, the nanocomposites show the following trend towards adsorption of MO: $G5_1P_1 > G4_1P_1 \approx G3_1P_1 >$ Fe_3O_4/P(NIPAM-*co*-MAA) microspheres

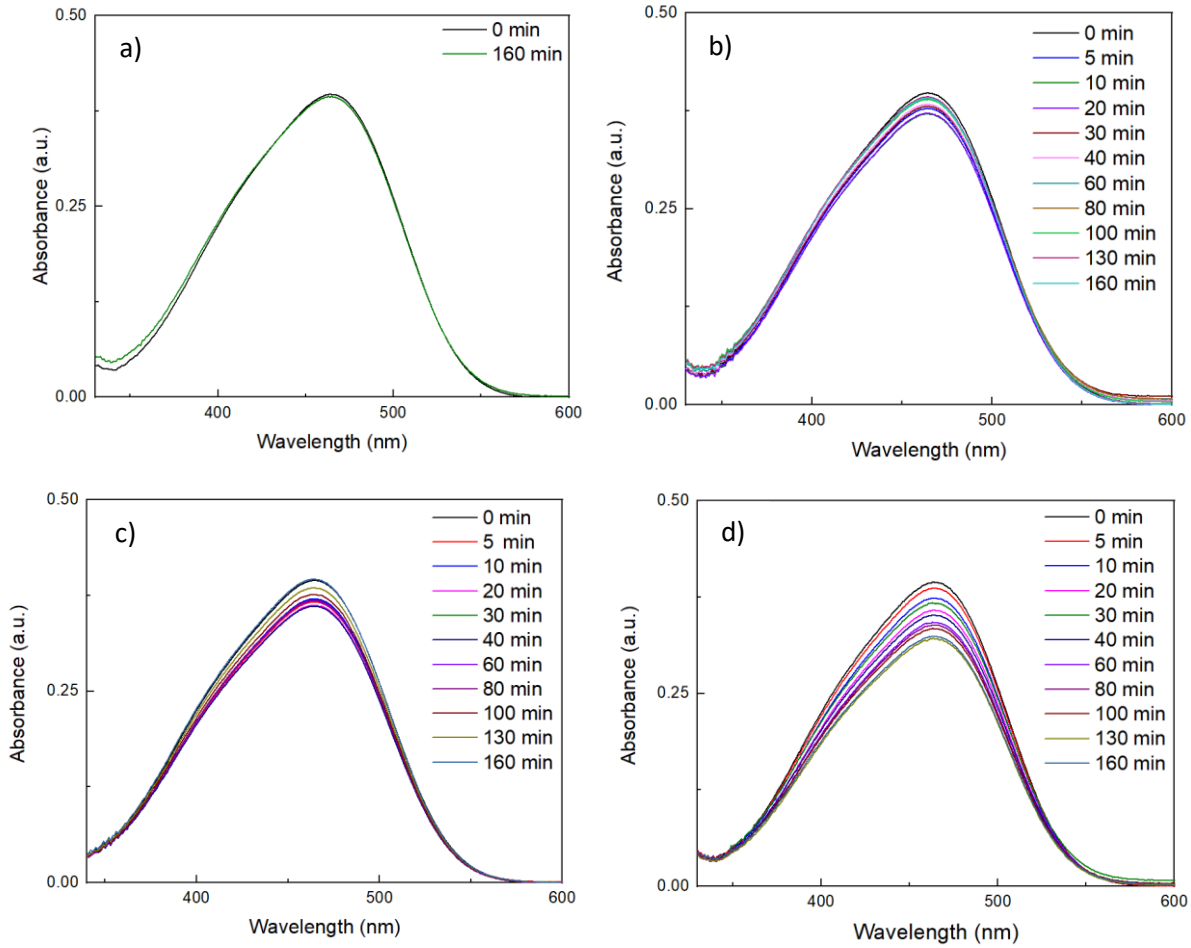

Figure 25: UV-Vis spectra of MO in the water at different times of the adsorption experiment testing by a) Fe_3O_4/P(NIPAM-*co*-MAA) microspheres, b) $G3_1P_1$, c) $G4_1P_1$,and d) $G5_1P_1$ nanocomposites

3.3.3 Adsorption of basic fuchsin and methyl orange with the PAMAM (G5) grafted-magnetic Fe_3O_4/P(NIPAM-*co*-MAA) nanocomposite and comparison between all nanocomposites

From the previous paragraphs, it can be concluded that G51P1 nanocomposite adsorbs both dyes (BF and MO) more efficiently than the other synthesized nanocomposites. In order to find the optimum nanocomposite structure to have the best adsorption properties, other nanocomposites were synthesized by using the PAMAM (G5) and changing the molar ratio of amino (dendrimer) to carboxylic (polymeric microspheres) groups during the synthesis. In particular, two kinds of nanocomposites (G51P05 and G51P08) were prepared by using a molar ratio respectively of 1:0.5 and 1:0.8 of amino to carboxylic groups. Once the nanocomposites were prepared, the adsorption experiments towards MO and BF were performed in aqueous solution. The initial concentration for both dyes is 0.015 mol/L, as in the previous experiments.

Figure 26 shows the UV-Vis spectra of BF at the different times of the adsorption experiment with the G51P05 and G51P08 nanocomposite. According to the experimental results, G51P05 nanocomposite does not adsorb BF efficiently; it could adsorb only 15% of BF at 30 minutes. However, G51P08 nanocomposite adsorbs BF much more efficiently than G51P05. The percentage of adsorption is 33.28% for BF at 20 minutes. This shows that when decreasing by half the quantity of polymeric microspheres in the nanocomposite, the adsorption properties against BF decrease drastically. Even a small decrease on the quantity of polymer in the nanocomposite, brings to a decrease of adsorption of BF in respect to the 1:1 nanocomposite. A trend can be observed showing that when increasing slightly the polymer content in the nanocomposites, the adsorption properties improve. Figure 26 shows the UV-Vis spectra of MO at the different times of the adsorption experiment with the G51P05 and G51P08 nanocomposite. The adsorption capacity of G51P05 is 25.25% and G51P08 is 23.14% for MO. So, the experimental results show that both nanocomposites adsorb MO slightly more than in the nanocomposites with a 1:1 molar ratio of amino to carboxylic groups.

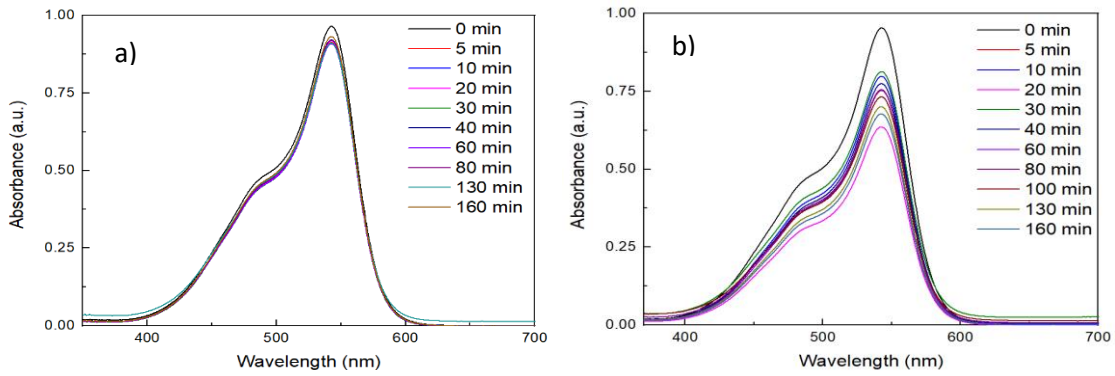

Figure 26: UV-Vis spectra of BF in water at different times of the adsorption experiment testing by a) $G5_1P_{05}$, b) $G5_1P_{08}$ nanocomposites

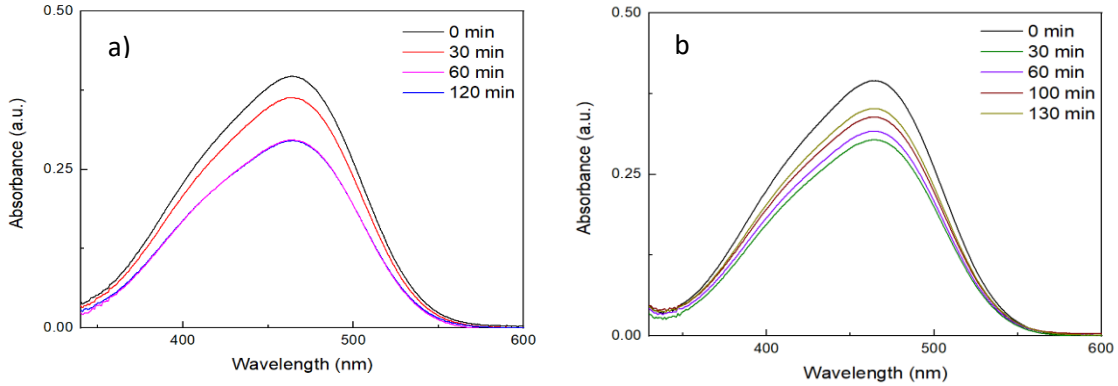

Figure 27: UV-Vis spectra of MO in water at different times of the adsorption experiment testing by a) $G5_1P_{05}$, b) $G5_1P_{08}$ nanocomposites

In conclusion, the most promising nanocomposite is the $G5_1P_1$ where the PAMAM (G5) is used and a 1:1 molar ratio of amino to carboxylic groups during the synthesis. To more deeply interpret the data for $G5_1P_1$ nanocomposite, the normalized concentration [C_t/C_0] of BF and MO was calculated by using a calibration curve (For calibration curves of BF and MO see Appendix). Figure 28 shows the normalized concentration of BF and MO versus time (min) when using the $G5_1P_1$nanocomposite.

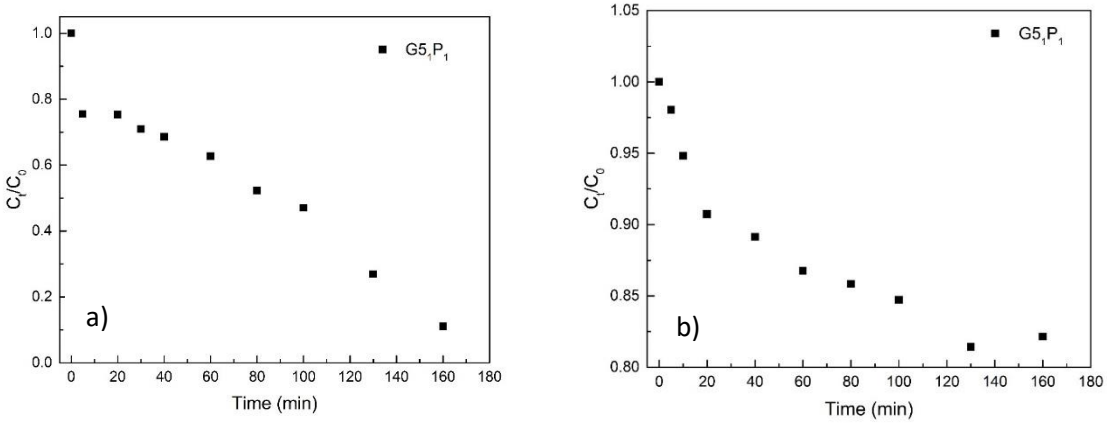

Figure 28: Adsorption vs time for a) BF and b) MO when using the nanocomposite $G5_1P_1$

To better compare the adsorption capacity of all nanocomposites prepared, the percentage of adsorbed dyes was calculated according to the given formula [6]. The same equation was used for each dye, and each nanomaterial used. By absorbance is intended the value of absorbance at the wavelength where the dye presents the maximum absorbance nm (the absorbance of BF at 542 nm; MO at 463 nm).

$$Adsorption(\%) = \frac{(First\ Absorbance - Last\ Absorbance)}{First\ Absorbance} * 100 \qquad [6]$$

In Table 4, all the adsorption capacities of the different nanocomposites and the Fe_3O_4/P(NIPAM-*co*-MAA) are compared. As discussed in the previous Sections, a trend is observed. For BF, the Fe_3O_4/P(NIPAM-*co*-MAA) and the $G5_1P_1$ are the materials that possess the best adsorption capacity. For MO, the three nanocomposites containing the PAMAM (G5) are the best performing materials. When the higher generation of PAMAM dendrimer is used, the number of amino groups in the nanocomposite is increasing. So, the nanocomposites should adsorb more negatively charged dyes from water. This is exactly what was observed in this work, but unexpectedly the $G5_1P_1$ adsorb very well also BF. Therefore, the novel nanocomposite is very promising for adsorption in wastewater treatment methods. Indeed, the adsorption towards BF

is not decreased and the one towards MO is considerably increased in respect to the polymeric microspheres. In addition, since the nanocomposite contains magnetic particles, in future its reusability could be investigated.

Table 4: Adsorption percentages of BF and MO when using Fe_3O_4/P(NIPAM-*co*-MAA) microspheres and the PAMAM dendrimer-grafted Fe_3O_4/P(NIPAM-*co*-MAA) nanocomposites

Samples	Adsorption (%) of BF	Adsorption (%) of MO
Fe_3O_4/P(NIPAM-*co*-MAA)	82.71	0
$G3_1P_1$	37.53	9.73
$G4_1P_1$	63.54	8.49
$G5_1P_1$	88.92	17.75
$G5_1P_{05}$	15.68	25.23
$G5_1P_{08}$	33.28	23.14

The adsorption kinetics were calculated in order to determine the adsorption rate of BF and MO by the synthesized nanocomposites and the polymeric microspheres. The experimental data were analysed and evaluated by using Lagergren pseudo-first-order and pseudo-second-order models (For the equation see section 2.3.2). Table 5 shows the kinetic constants and parameters of the most promising nanocomposite $G5_1P_1$.

Figure 29 and 30 show respectively; pseudo-first and second-order models fitting for the adsorption of BF by the nanocomposite $G5_1P_1$. Figure 31 and 32 show respectively; the pseudo-first and second order models for the adsorption of MO by the nanocomposite $G5_1P_1$.

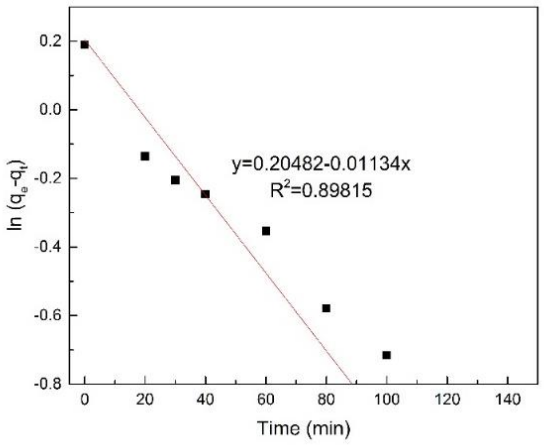

Figure 29: Pseudo-first-order model fitting for the adsorption of BF by the nanocomposite $G5_1P_1$

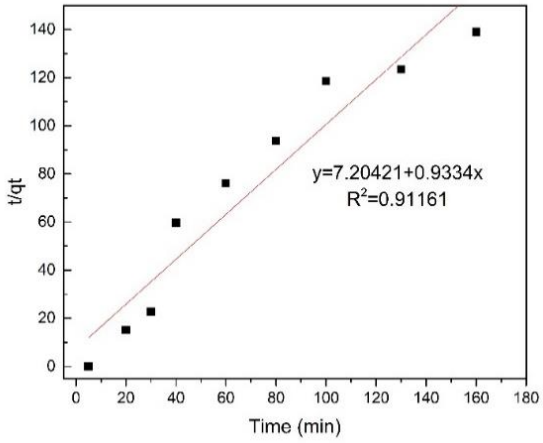

Figure 30: Pseudo-second-order model fitting for the adsorption of BF by the nanocomposite $G5_1P_1$

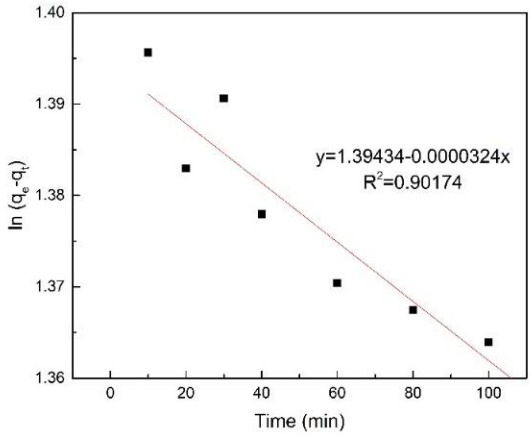

Figure 31: Pseudo-first-order model fitting for the adsorption of MO by the nanocomposite $G5_1P_1$

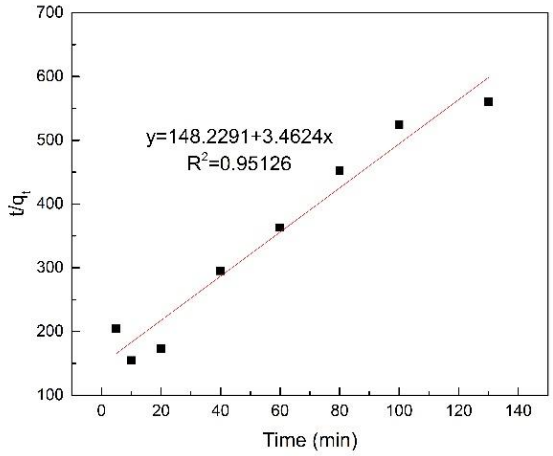

Figure 32: Pseudo-second-order model fitting for the adsorption of MO by the nanocomposite $G5_1P_1$

Table 5: Pseudo-first-order and Pseudo-second-order model parameters of adsorption kinetics of BF and MO

Dyes	Samples	Pseudo-first-order model				Pseudo-second-order model		
		$q_{e,exp}$ [mg g^{-1}]	q_e [mg g^{-1}]	k_1 [mim^{-1}]	R^2	q_e [mg g^{-1}]	k_2 [mim^{-1}]	R^2
BF	$G5_1P_1$	1.208625	1.2273	0.01134	0.89815	1.0713	0.01798	0.91161
MO	$G5_1P_1$	4.102312	4.03231	0.00003	0.90174	0.2888	0.00015	0.95126

The adsorption kinetic curve of $G5_1P_1$ shows a better fitting with the pseudo-second-order model than the pseudo-first-order model.

Chapter 4

4. Conclusions

Nowadays, industrial activities, such as textile, produce big amounts of dyes that are released in water. Dyes create huge environmental problems and threat animal and human health. In particular, azo dyes are highly toxic, resistant and particularly hard to degrade because they contain nitrogen-nitrogen double bonds. In addition, in wastewater differently charged dyes can be present. Removing these pollutants with a single method or material is hard by using traditional treatment techniques.

In this study, novel nanocomposites able to remove differently charged dyes have been prepared. In particular, polymeric magnetic microspheres, namely Fe_3O_4/P(NIPAM-*co*-MAA), and different generations of Polyamidoamine (PAMAM) dendrimers were combined to obtain these nanocomposites. The prepared nanocomposites can adsorb differently charged dyes and can also be removed thanks to their magnetic properties. The nanocomposites were tested for the adsorption of the positively charged dye basic fuchsin (BF) and the negatively charged azo dye methyl orange (MO). The nanocomposites that showed the best performance in the adsorption experiments were also prepared by changing the molar ratio of polymer/dendrimer to explore more in-depth their adsorption properties.

Section 1 a comprehensive introduction on the state-of-the-art about water pollution, water treatment methods, adsorption, polymeric microspheres and dendrimers for wastewater treatment is presented.

Section 2 consists of a description of the materials and methods used. In particular, it is explained how the nanocomposites were prepared, characterized, and how the adsorption tests towards BF and MO were performed. This Section also contains a short explanation of the principles of the main techniques used. The nanocomposites were prepared by forming a chemical bond between the carboxylic groups of the magnetic Fe_3O_4/P(NIPAM-*co*-MAA) microspheres and the amino groups of the PAMAM dendrimers. Different nanocomposites were prepared by changing the generation of the dendrimer used or by changing the molar ratio between the polymer and the dendrimer. In particular, 5 different kinds of nanocomposites were prepared. Three nanocomposites were prepared, respectively, by coupling the 3rd, 4th and 5th generations of PAMAM dendrimers to the Fe_3O_4/P(NIPAM-*co*-MAA) microspheres in a 1:1 molar ratio of amino groups to carboxylic groups. These nanocomposites were called $G3_1P_1$, $G4_1P_1$ and $G5_1P_1$ (See the details in the 2.1.2 section) depending if the generation of the dendrimer used was, respectively, the 3rd, 4th or 5th. The two other nanocomposites were prepared by using a different molar ratio of amino groups (in the dendrimer) to carboxylic

groups (in the microspheres), but keeping the same dendrimer generation, PAMAM (G5). The molar ratio 1:05 and 1:08 of amino groups to carboxylic groups were used for the synthesis of $G5_1P_{05}$ and $G5_1P_{08}$ nanocomposites.

In Section 3, the results and discussion are reported. In particular, after a session about the nanocomposites characterization, the adsorption tests of the nanocomposites towards BF and MO are discussed. The nanocomposites were characterized by ATR-FTIR spectroscopy, UV-Vis spectroscopy, DLS measurements and HR-TEM measurements. The characterization shows that both the dendrimer and the polymeric microspheres are present in the nanocomposite and that the size of the nanocomposite does not seem to change dramatically in comparison to the size of the microspheres.

The nanocomposites were then used for the adsorption experiments of BF and MO in comparison to the non-modified polymeric microspheres. The adsorption experiments were performed for 160 minutes in the dark and at room temperature. Aliquots of the dye solution were collected at different times of the adsorption experiment and measured by UV-Vis spectroscopy to evaluate the decrease of the absorbance intensity in time. The results showed that there is a relationship between the generations of PAMAM dendrimer used in the nanocomposite and the adsorption rate and efficiency. When higher generations of PAMAM dendrimer are used for the synthesis of the nanocomposites, the adsorption of both BF and MO is better than with the nanocomposites synthesized using lower generations of PAMAM dendrimers.

According to the obtained results, the ideal nanocomposite was determined to be $G5_1P_1$. In order to find the optimum molar ratio of polymeric microspheres/dendrimers in the nanocomposite, other two syntheses were performed by changing the molar ratio between the amino groups of the dendrimer and the carboxylic groups of the polymeric microspheres during the synthesis (as explained above). The adsorption capacity of BF by the obtained nanocomposites $G5_1P_{05}$ and $G5_1P_{08}$ drops drastically in respect to $G5_1P_1$ nanocomposite. However, $G5_1P_{05}$ and $G5_1P_{08}$ adsorb MO slightly better than $G5_1P_1$ nanocomposite.

MO is a negatively charged dye and BF is a positively charged dye. When the higher generation of PAMAM dendrimer is used, the number of available amino groups in the nanocomposites is increasing. This means that $G5_1P_1$ contains more amino groups than $G4_1P_1$ that contains more amino groups than $G3_1P_1$ nanocomposites. Therefore, the adsorption of MO is expected to increase by increasing the dendrimer generation. This is, indeed, in perfect line with what has been found in this work. When the dendrimer generation increases, theoretically the adsorption

capacity towards BF should decrease as well, in respect of when using the only polymeric microspheres. This has been observed for the nanocomposites $G3_1P_1$ and $G4_1P_1$. When using $G5_1P_1$, the adsorption of BF is equally good as with the only polymeric microsphere. Further studies and investigations are required to understand why, but the $G5_1P_1$ is a very promising nanocomposite since it can adsorb very well both MO and BF and can also be recycled thanks to the magnetic properties.

In conclusion, $G5_1P_1$ nanocomposite is a promising novel material able to adsorb oppositely charged dyes such as MO and BF from water. Indeed, in respect to the polymeric microspheres, the adsorption towards BF is not decreased and the one towards MO is considerably increased. Because of the magnetic properties of the new nanocomposite, in future, its removal from water and its reusability could be investigated.

5. References:

(1) Hornyak, G. L.; Tibbals, H. F.; Dutta, J.; Moore, J. J. Introduction to Nanoscience and Nanotechnology. In *Introduction to Nanoscience and Nanotechnology*; CRS press Taylor&Francis Group, 2009; pp 1483–1567.

(2) Ali Mansoori, G.; Bastami, T. R.; Ahmadpour, A.; Eshaghi, Z. Environmental Application of Nanotechnology. In *Annual Review of Nano Research Guozhong Cao (University of Washington, USA) and C Jeffrey Brinker (University of New Mexico & Sandia National Laboratories, USA)*; Annual Review of Nano Research; WORLD SCIENTIFIC, 2008; Vol. 2, pp 439–493. https://doi.org/doi:10.1142/9789812790248_0010.

(3) Goel, A. Impact of Nanotechnology on Environment. *BioEvolution* **2014**, 42–45.

(4) Picó, Y.; Barceló, D. Analysis and Prevention of Microplastics Pollution in Water: Current Perspectives and Future Directions. *ACS Omega* **2019**, *4*, 6709–6719. https://doi.org/10.1021/acsomega.9b00222

(5) A.Alrumman, S.; El-kott, A.; Keshk, S. M. A. . Water Pollution : Source & Treatment. *Am. J. Environ. Eng.* **2016**, *6*, 88–98. https://doi.org/10.5923/j.ajee.20160603.02.

(6) Omer, A.; Baker, B. H.; Aldridge, C. A. *Water: Availability and Use*; **2016**,11-16. https://doi.org/10.1007/978-3-662-10868-0_19.

(7) Shukla, D.; Vaghela, Krishnakumar B, Jain, Nayan, Mishra, A. Impact of Pollution on Aquatic Fauna of River Ecosystem: A Review. *Int. J. Curr. Adv. Res.* **2017**, *6*, 6518–6524. https://doi.org/10.24327/ijcar.2017.6524.0957.

(8) Pathak, J. Causes , Effects and Control of Water Pollution in India. *Int. J. Acad. Res. Dev.* **2018**, *3*, 939–942.

(9) The World Bank. The Bangladesh Responsible Sourcing Initiative, A New Model For Green Growth. *Bangladesh Responsible Sourc. Initiat. A New Model Green Growth* **2014**, *1*, 1–80.

(10) Hassaan, M. A.; Nemr, A. El. Health and Environmental Impacts of Monsanto's Roundup Pesticide. *Org. Consum. Assoc.* **2017**, *(1)3*, 64–67.

(11) Madhav, S.; Ahamad, A.; Singh, P.; Mishra, P. K. A Review of Textile Industry: Wet Processing, Environmental Impacts, and Effluent Treatment Methods. *Environ. Qual. Manag.* **2018**, *27*, 31–41. https://doi.org/10.1002/tqem.21538.

(12) Sivri, N.; Toroz, İ.; Tüfekci, N. Pollutants of Textile Industry Wastewater and Assessment of Its Discharge Limits by Water Quality Standards. *Turkish J. Fish. Aquat. Sci.* **2007**, *7*, 97–103.

(13) Shanker, U.; Rani, M.; Jassal, V. Degradation of Hazardous Organic Dyes in Water by Nanomaterials. *Environ. Chem. Lett.* **2017**, *15*, 623–642. https://doi.org/10.1007/s10311-017-0650-2.

(14) Gita, S.; Hussan, A.; Choudhury, T. G. Impact of Textile Dyes Waste on Aquatic Environments and Its Treatment. *Environ. Ecol.* **2017**, *35*, 2349–2353.

(15) Tatarko, M.; Tricker, J.; Andrzejewski, K.; Bumpus, J. A.; Rhoads, H. Remediation of Water Contaminated with an Azo Dye: An Undergraduate Laboratory Experiment Utilizing an Inexpensive Photocatalytic Reactor. *J. Chem. Educ.* **2009**, *76*, 1680–1683. https://doi.org/10.1021/ed076p1680.

(16) Rasalingam, S.; Peng, R.; Koodali, R. T. Removal of Hazardous Pollutants from Wastewaters:Applications of TiO2-SiO2 Mixed Oxide Materials. *J. Nanomater.* **2014**, *2014*, 1–42. https://doi.org/10.1155/2014/617405

(17) Hoffman, D.J.; Rattner, B.A.; Burton, G.A.; Cairns, J.,*Handbook of Ecotoxicology*, 2nd ed., CRC Press LLC, United States of America,**2003**, 313–340.

(18) Yaseen, D. A.; Scholz, M. Treatment of Synthetic Textile Wastewater Containing Dye Mixtures with Microcosms. *Environ. Sci. Pollut. Res.* **2018**, *25*, 1980–1997. https://doi.org/10.1007/s11356-017-0633-7.

(19) Zaharia, C.; Suteu, D.; Muresan, A.; Muresan, R.; Popescu, A. Textile Wastewater Treatment by Homogeneous Oxidation with Hydrogen Peroxide. *Environ. Eng. Manag. J.* **2009**, *8*, 1359–1369. https://doi.org/10.30638/eemj.2009.199

(20) Tami, K.; Popova, A.; Proni, G. Engaging Students in Real-World Chemistry through Synthesis and Confirmation of Azo Dyes via Thin Layer Chromatography To Determine the Dyes Present in Everyday Foods and Beverages. *J. Chem. Educ.* **2017**, *94*, 471–475. https://doi.org/10.1021/acs.jchemed.6b00334.

(21) Mathew, B. B.; Krishnamurthy, N. B. Water: Its Constituents and Treatment Methods. *Artic. J. Renew. Sustain. Energy* **2014**, *1*, 21–28. https://doi.org/10.12966/rse.09.02.2014.

(22) Jaishankar, M.; Tseten, T.; Anbalagan, N.; Mathew, B. B.; Beeregowda, K. N. Toxicity,

Mechanism and Health Effects of Some Heavy Metals. *Interdiscip. Toxicol.* **2014**, *7*, 60–72. https://doi.org/10.2478/intox-2014-0009.

(23) Shekhawat, K.; Chatterjee, S.; Joshi, B. Chromium Toxicity and Its Health Hazards. *Int. J. Adv. Res.* **2015**, *3*, 167–172.

(24) Sarkar, S.; Banerjee, A.; Halder, U.; Biswas, R. Degradation of Synthetic Azo Dyes of Textile Industry : A Sustainable Approach Using Microbial Enzymes. *Water Conserv. Sci. Eng.* **2017**, *2*, 121–131. https://doi.org/10.1007/s41101-017-0031-5.

(25) Gong, R.; Ye, J.; Dai, W.; Yan, X.; Hu, J.; Hu, X.; Li, S.; Huang, H. Adsorptive Removal of Methyl Orange and Methylene Blue from Aqueous Solution with Finger-Citron-Residue-Based Activated Carbon. *Ind. Eng. Chem. Res.* **2013**, *52*, 14297–14303. https://doi.org/10.1021/ie402138w.

(26) Seredych, M.; Bandosz, T. J. Removal of Cationic and Ionic Dyes on Industrial-Municipal Sludge Based Composite Adsorbents. *Ind. Eng. Chem. Res.* **2007**, *46*, 1786–1793. https://doi.org/10.1021/ie0610997.

(27) Vutskits, L.; Briner, A.; Klauser, P.; Gascon, E.; Dayer, A. G.; Kiss, J. Z.; Muller, D.; Licker, M. J.; Morel, D. R. Adverse Effects of Methylene Blue on the Central Nervous System. *Anesthesiology,* **2008**, *108*, 684–692. https://doi.org/10.1097/ALN.0b013e3181684be4.

(28) Ning, J.; Wang, M.; Luo, X.; Hu, Q.; Hou, R.; Chen, W.; Chen, D.; Wang, J.; Liu, J. SiO_2 Stabilized Magnetic Nanoparticles as a Highly Effective Catalyst for the Degradation of Basic Fuchsin in Industrial Dye Wastewaters. *Molecules,* **2018**, *23*, 1–16. https://doi.org/10.3390/molecules23102573.

(29) Samarghandi, M. R.; Hadi, M.; Moayedi, S.; Askari, F. B. Two-Parameter Isotherms of Methyl Orange Sorption by Pinecone Derived Activated Carbon. *Iranian J. Environ. Health Sci. Eng.* **2009**, *6*, 285–294.

(30) Worch, E. Adsorption Technology in Water Treatment Fundamentals, Processes, and Modeling. *Adsorpt. Technol. Water Treat. Fundam. Process. Model.* **2012**, 11–34.

(31) Ali, I.; Asim, M.; Khan, T. A. Low Cost Adsorbents for the Removal of Organic Pollutants from Wastewater. *J. Environ. Manage.* **2012**, *113*, 170–183. https://doi.org/10.1016/j.jenvman.2012.08.028.

(32) United States, Environmental Protection Agency, O. of W. M. Primer for Municipal Wastewater Treatment Systems. *Prim. Munic. wastewater Treat. Syst.* **2004**, 1–30.

(33) Shankar, U.; Uday, P.; Mahata, N.; Sasmal, S.; Mondal, A. *Dyes Contamination in the Environment: Ecotoxicological Effects, Health Hazards, and Biodegradation and Bioremediation Mechanisms for Environmental Cleanup*; 2017.

(34) Paridah, M. .; Moradbak, A.; Mohamed, A. .; Owolabi, F. abdulwahab taiwo; Asniza, M.; Abdul Khalid, S. H. . Adsorption Technique for the Removal of Organic Pollutants from Water and Wastewater. In *Organic Pollutants - Monitoring, Risk and Treatment Efficient*; 2013; pp 167–194.

(35) Bonilla-petriciolet, A.; Mendoza-castillo, D. I. Adsorption Processes for Water Treatment and Purification. *Adsorpt. Process. Water Treat. Purif.* **2017**, 230–238.

(36) Tantra, R. *Nanomaterial Characterization An Introduction*; John Wiley& Sons, Inc.,Hoboken,New Jersey: Canada, 2016.

(37) Sadegh, H.; Ali, G. A. M.; Gupta, V. K. The Role of Nanomaterials as Effective Adsorbents and Their Applications in Wastewater Treatment. *J. Nanostructure Chem.* **2017**, *7:1*, 1–14. https://doi.org/10.1007/s40097-017-0219-4.

(38) Milowska, K. Z.; Majewski, J. A. Functionalization of Carbon Nanotubes with -CHn, -NHnfragments, -COOH and -OH Groups. *J. Chem. Phys.* **2013**, *138*, 1–13. https://doi.org/10.1063/1.4804652

(39) Iijima, S. Helical Microtubules of Graphitic Carbon. *Nature* **1991**, *354*, 56–58.

(40) Andrews, R.; Jacques, D.; Qian, D.; Rantell, T. Multiwall Carbon Nanotubes : Synthesis and Application. *Acc. Chem. Res.* **2002**, *35*, 1008–1017. https://doi.org/10.1021/ar010151m.

(41) Alshehri, R.; Ilyas, A. M.; Hasan, A.; Arnaout, A.; Ahmed, F.; Memic, A. Carbon Nanotubes in Biomedical Applications : Factors , Mechanisms , and Remedies of Toxicity. *J. Med. Chem.* **2016**, *59*, 8149–8167. https://doi.org/10.1021/acs.jmedchem.5b01770.

(42) Huang, D.; Li, B.; Wu, M.; Kuga, S.; Huang, Y. Graphene Oxide-Based Fe-Mg (Hydr)Oxide Nanocomposite as Heavy Metals Adsorbent. *J. Chem. Eng. Data* **2018**, *63*, 2097–2105. https://doi.org/10.1021/acs.jced.8b00100.

(43) Yavuz, E.; Tokalıoğlu, Ş.; Şahan, H.; Patat, Ş. A Graphene/Co_3O_4 Nanocomposite as a New Adsorbent for Solid Phase Extraction of Pb(II), Cu(II) and Fe(III) Ions in Various Samples. *RSC Advances,* **2013**, *3*, 24650–24657. https://doi.org/10.1039/c3ra45111a.

(44) Xu, P.; Ming, G.; Lian, D.; Ling, C.; Hu, S.; Hua, M. Use of Iron Oxide Nanomaterials in

Wastewater Treatment: A Review. *Sci. Total Environ.* **2012**, *424*, 1–10. https://doi.org/10.1016/j.scitotenv.2012.02.023.

(45) Ramirez Leyva, J. H.; Hethnawi, A.; Vitale, G.; Nassar, N. N. Magnetic Nanostructured White Graphene for Oil Spill and Water Cleaning. *Ind. Eng. Chem. Res.* **2018**, *57*, 13065–13076. https://doi.org/10.1021/acs.iecr.8b02785.

(46) Huang, L.; Peng, C.; Cheng, Q.; He, M.; Chen, B.; Hu, B. Thiol-Functionalized Magnetic Porous Organic Polymers for Highly Efficient Removal of Mercury. *Ind. Eng. Chem. Res.* **2017**, *56*, 13696–13703. https://doi.org/10.1021/acs.iecr.7b03093.

(47) Ambashta, R. D.; Sillanpää, M. Water Purification Using Magnetic Assistance : A Review. *J. Hazard. Mater.* **2010**, *180*, 38–49. https://doi.org/10.1016/j.jhazmat.2010.04.105.

(48) Sharma, R. K.; Monga, Y.; Puri, A.; Gaba, G. Magnetite (Fe_3O_4) Silica Based Organic–Inorganic Hybrid Copper(II) Nanocatalyst: A Platform for Aerobic N-Alkylation of Amines†. *Green Chem.* **2013**, *15*, 2800–2809.

(49) Zhang, S.; Zhang, Y.; Liu, J.; Xu, Q.; Xiao, H.; Wang, X.; Xu, H. Thiol Modified Fe_3O_4@SiO_2 as a Robust, High Effective, and Recycling Magnetic Sorbent for Mercury Removal. *Chem. Eng. J.* **2013**, *226*, 30–38.https://doi.org/10.1016/j.cej.2013.04.060.

(50) Yang, M.; Huang, Y.; Yue, Q.; Cao, H.; Li, X.; Lin, Y. Preparation of a Novel Polymeric Adsorbent and Its Adsorption of Phenol in Aqueous Solution. *Desalin. Water Treat.* **2016**, *57*, 13295-13306. https://dx.doi.org/10.1080/19443994.2015.1055814.

(51) Kolya, H.; Das, S.; Tripathy, T. Synthesis of Starch-g-Poly-(N-Methylacrylamide-Co-Acrylic Acid) and Its Application for the Removal of Mercury (II) from Aqueous Solution by Adsorption. *Eur. Polym. J.* **2014**, *58*, 1–10.

(52) Opoku, F.; Kiarii, M. E.; Governder, P. P.; Mano, M. A. Descriptive Inorganic Chemistry Researches of Metal Compounds. In *Descriptive Inorganic Chemistry Researches of Metal Compounds*; 2017; pp 174–199.

(53) Zhao, G.; Huang, X.; Tang, Z.; Huang, Q.; Niu, F.; Wang, X. Polymer-Based Nanocomposites for Heavy Metal Ions Removal from Aqueous Solution: A Review. *Polym. Chem.* **2018**, *9*, 3562–3582. https://doi.org/10.1039/c8py00484f.

(54) Wang, J.; Zhang, W.; Qian, Y.; Deng, B.; Tian, W. pH, Temperature, and Magnetic Triple-Responsive Polymer Porous Microspheres for Tunable Adsorption. *Macromol. Mater. Eng.* **2016**, *301*, 1132–1141. https://doi.org/10.1002/mame.201600161.

(55) Feldman, H. J.; Dumontier, M.; Ling, S.; Haider, N.; Hogue, C. W. V. CO: A Chemical Ontology for Identification of Functional Groups and Semantic Comparison of Small Molecules. *FEBS Lett.* **2005**, *579*, 4685–4691. https://doi.org/10.1016/j.febslet.2005.07.039.

(56) Wang, B.; Bai, Z.; Jiang, H.; Prinsen, P.; Luque, R.; Zhao, S.; Xuan, J. Selective Heavy Metal Removal and Water Purification by Microfluidically-Generated Chitosan Microspheres: Characteristics, Modeling and Application. *J. Hazard. Mater.* **2019**, *364*, 192–205. https://doi.org/10.1016/j.jhazmat.2018.10.024.

(57) Hu, J. L.; Luo, L. B.; Yang, X. Z.; Yao, R. S.; Zhang, H. Bin; Qian, H. S. Silica-Based Hybrid Microspheres: Synthesis, Characterization and Wastewater Treatment. *RSC Adv.* **2013**, *3*, 25620–25626. https://doi.org/10.1039/c3ra44111c.

(58) Zdravkovic, A.; Nikolic, L.; Ilic-Stojanovic, S.; Nikolic, V. The Application of Hydrogels Based on N-Isopropylacrylamide and Anionic Comonomers. *Adv. Technol.* **2017**, *6*, 33–44. https://doi.org/10.5937/savteh1701033z.

(59) Abbasi, E.; Aval, S.F.; Akbarzadeh, A.; Milani, M.; Nasrabadi, H.T.; Joo, S.W.; Hanifehpour, Y.; Nejati-Koshki, K.; Pashaei-Asl, R. Dendrimers: Synthesis, Applications, and Properties. *Nanoscale Res. Lett.* **2014**, *9*, 1–10.

(60) Maiti, P. K.; Çağin, T.; Wang, G.; Goddard, W. A. Structure of PAMAM Dendrimers: Generations 1 through 11. *Macromolecules* **2004**, *37*, 6236–6254. https://doi.org/10.1021/ma035629b.

(61) Prasanna, P. R.; Selvamani, P.; Gomathi, E. Waste Water Treatment Through Dendrimer – Conjugated Magnetic Nanoparticles. *Int. J. ChemTech Res.* **2013**, *5*, 1239–1245.

(62) Wiesler, U. M.; Berresheim, A. J.; Morgenroth, F.; Lieser, G.; Müllen, K. Divergent Synthesis of Polyphenylene Dendrimers: The Role of Core and Branching Reagents upon Size and Shape. *Macromolecules* **2001**, *34*, 187–199. https://doi.org/10.1021/ma991519m.

(63) Shadrack, D. M.; Mubofu, E. B.; Nyandoro, S. S. Synthesis of Polyamidoamine Dendrimer for Encapsulating Tetramethylscutellarein for Potential Bioactivity Enhancement. *Int. J. Mol. Sci.* **2015**, *16*, 26363–26377. https://doi.org/10.3390/ijms161125956.

(64) Asthana, A.; Chauhan, A. S.; Diwan, P. V.; Jain, N. K. Poly(Amidoamine) (PAMAM) Dendritic Nanostructures for Controlled Sitespecific Delivery of Acidic Anti-Inflammatory

Active Ingredient. *AAPS PharmSciTech* **2005**, *6*, E536–E542. https://doi.org/10.1208 / pt060367.

(65) Santos, S. D.; Xavier, M.; Leite, D. M.; Moreira, D. A.; Custódio, B.; Torrado, M.; Castro, R.; Leiro, V.; Rodrigues, J.; Tomás, H.; et al. PAMAM Dendrimers: Blood-Brain Barrier Transport and Neuronal Uptake after Focal Brain Ischemia. *J. Control. Release* **2018**, *291*, 65–79. https://doi.org/10.1016/j.jconrel.2018.10.006.

(66) Sajid, M.; Khaled, M.; Baig, N. Removal of Heavy Metals and Organic Pollutants from Water Using Dendritic Polymers Based Adsorbents : A Critical Review. *Seperation Purif. Technol. 191* **2018**, *191*, 400–423. https://doi.org/10.1016/j.seppur.2017.09.011.

(67) Aliannejadi, S.; Hassani, A. H.; Panahi, H. A.; Borghei, S. M. Fabrication and Characterization of High-Branched Recyclable PAMAM Dendrimer Polymers on the Modified Magnetic Nanoparticles for Removing Naphthalene from Aqueous Solutions. *Microchem. J.* **2019**, *145*, 767–777. https://doi.org/10.1016/j.microc.2018.11.043.

(68) Diallo, M. S. Water Treatment by Dendrimer-Enhanced Filtration : Principles and Applications. In *Nanotechnology Applications for Clean Water*; Street, A., Sustich, R., Duncan, J., Savage, N., Eds.; William Andrew, 2009; pp 143–155. https://doi.org/10.1016/B978-0-8155-1578-4.50020-2.

(69) Peng, X. C.; Peng, X. H.; Liu, S. M.; Zhao, J. Q. Synthesis and Properties of New Amphoteric Poly(Amidoamine) Dendrimers. *Express Polym. Lett.* **2009**, *3*, 510–517. https://doi.org/10.3144/expresspolymlett.2009.63.

(70) Klajnert, B.; Bryszewska, M. Dendrimers : Properties and Applications. *Rev. Lit. Arts Am.* **2001**, *48*, 199–208. https://doi.org/10.1016/B978-0-444-53349-4.00162-X.

(71) Chaudhuri, C. R.; Chatterjee, S. N. Release of P-32 Compounds from Labelled Vibrio Cholerae and Vibrio El Tor in Ethanol. *Bull. Calcutta Sch. Trop. Med.* **1969**, *17*, 5–6.

(72) Zhong, T.; Ai, P.; Zhou, J. Structures and Properties of PAMAM Dendrimer: A Multi-Scale Simulation Study. *Fluid Phase Equilib.* **2011**, *302*, 43–47. https://doi.org/10.1016/j.fluid.2010.09.037.

(73) Castro, R. M. de. DNA/Dendrimer-Based Films A Novel Material with Potential Biomedical Applications, Ph. D. Thesis, Madeira University, 2018.

(74) Kommu, A.; Velachi, V.; Cordeiro, M. N. D. S.; Singh, J. K. Removal of Pb(II) Ion Using PAMAM Dendrimer Grafted Graphene and Graphene Oxide Surfaces: A Molecular

Dynamics Study. *J. Phys. Chem. A* **2017**, *121*, 9320–9329. https://doi.org/10.1021/acs.jpca.7b09766.

(75) Sadeghi, S.; Raki, G.; Amini, A.; Mengelizadeh, N.; Amin, M. M. Study of the Effectiveness of the Third Generation Polyamide- Amine and Polypropylene Imine Dendrimers in Removal of Reactive Blue 19 Dye from Aqueous Solutions. *Environ. Heal. Eng. Manag. J.* **2018**, *5*, 197–203. https://doi.org/10.15171/EHEM.2018.27.

(76) Yagub, M. T.; Sen, T. K.; Afroze, S.; Ang, H. M. Dye and Its Removal from Aqueous Solution by Adsorption: A Review. *Adv. Colloid Interface Sci.* **2014**, *209*, 172–184. https://doi.org/10.1016/j.cis.2014.04.002.

(77) Feng, H.; Zhang, R.; Yang, X. Synthesis of P(MBA-Co-MAA) Microsphere-Grafted PAMAM Dendrimers and Their Application as Supporters for Gold Nanoparticles. *Colloid Polym. Sci.* **2013**, *291*, 1329–1339. https://doi.org/10.1007/s00396-012-2863-z.

(78) Charles, S.; Vasanthan, N.; Kwon, D.; Sekosan, G.; Ghosh, S. Surface Modification of Poly(Amidoamine) (PAMAM) Dendrimer as Antimicrobial Agents. *Tetrahedron Lett.* **2012**, *53*, 6670–6675. https://doi.org/10.1016/j.tetlet.2012.09.098.

(79) Y.S. Ho. Citation Review of Lagergren Kinetic Rate Equation on Adsorption Reactions. *Scientometrics* **2004**, *59*, 171–177. https://doi.org/10.1023/B:SCIE.0000013305.99473.cf.

(80) Gandomi, Y. A.; Aaron, D. S.; Houser, J. R.; Daugherty, M. C.; Clement, J. T.; Pezeshki, A. M.; Ertugrul, T. Y.; Moseley, D. P.; Mench, M. M. Critical Review—Experimental Diagnostics and Material Characterization Techniques Used on Redox Flow Batteries. *J. Electrochem. Soc.* **2018**, *165*, A970–A1010. https://doi.org/10.1149/2.0601805jes.

(81) Perkampus, H. H. UV-Vis Spectroscopy and Its Applications. *UV-Vis Spectrosc. Its Appl.* **1992**, 1–237.

(82) Schuttlefield, J. D.; Grassian, V. H. ATR–FTIR Spectroscopy in the Undergraduate Chemistry Laboratory. Part I: Fundamentals and Examples. *J. Chem. Educ.* **2009**, *85*, 279. https://doi.org/10.1021/ed085p279.

(83) Rytwo, G.; Zakai, R.; Wicklein, B. The Use of ATR-FTIR Spectroscopy for Quantification of Adsorbed Compounds. *J. Spectrosc.* **2015**, *2015*, 1–8. https://doi.org/10.1155/2015/727595.

(84) Stetefeld, J.; McKenna, S. A.; Patel, T. R. Dynamic Light Scattering: A Practical Guide and

Applications in Biomedical Sciences. *Biophys. Rev.* **2016**, *8*, 409–427. https://doi.10.1007/s12551-016-0218-6.

(85) Carvalho, P. M.; Felício, M. R.; Santos, N. C.; Gonçalves, S.; Domingues, M. M. Application of Light Scattering Techniques to Nanoparticle Characterization and Development. *Front. Chem.* **2018**, *6*, 1–17. https://doi:10.3389/fchem.2018.00237.

(86) Kumar, D. Co-Functionalised Gold Nanoparticles for Drug Delivery Applications Co-Functionalised Gold Nanoparticles for Drug Delivery Applications, University of Ulster, 2017. https://doi.org/10.13140/RG.2.2.30584.44800.

(87) Laboratories, H. L. H.; Carolina, S.; Douglas, J. F. Generalized Stokes-Einstein Equation for Spherical Particles Suspensions. *Pysical R* **1995**, *51*, 1081–1090.

(88) Reza, M.; Kontturi, E.; Jääskeläinen, A.; Vuorinen, T. Transmission Electron Microscopy for Wood and Fiber. *BioResources* **2015**, *10*, 6230–6261. https://doi.org/10.15376/biores.10.3.6230-6261.

(89) Suvorova, E. I.; Stadelmann, P. A.; Buffat, P.-A. HRTEM Simulation in Determination of Thickness and Grain Misorientation for Hydroxyapatite Crystals. *Crystallogr. Reports* **2004**, *49*, 343–352. https://doi.org/10.1134/1.1756632.

(90) Mundiña-, C.; Romero, E. L.; Morilla, M. J. Selective Cytotoxicity of PAMAM G5 on Melanoma Cells. *Int. J. Nanomedicine,* **2012**, *7*, 4121–4133. https://doi.org/10.2147/IJN.S32785.

(91) Torigoe, K.; Suzuki, A.; Esumi, K. Au(III)-PAMAM Interaction and Formation of Au-PAMAM Nanocomposites in Ethyl Acetate. *J. Colloid Interface Sci.* **2001**, *241*, 346–356. https://doi.org/10.1006/jcis.2001.7778.

APPENDIX

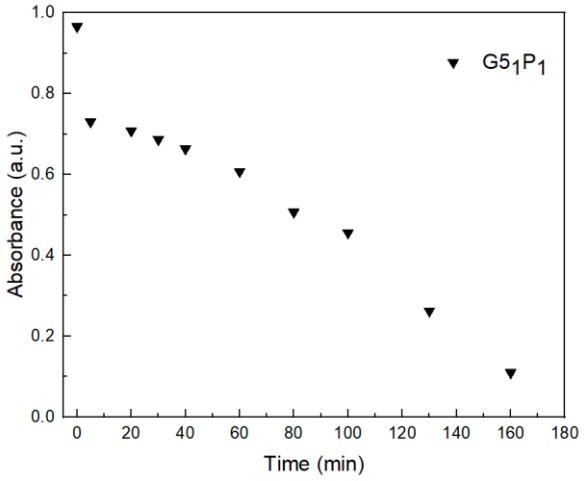

Figure A1: Absorbance versus time (min) graph of BF during the adsorption experiment with the nanocomposite $G5_1P_1$

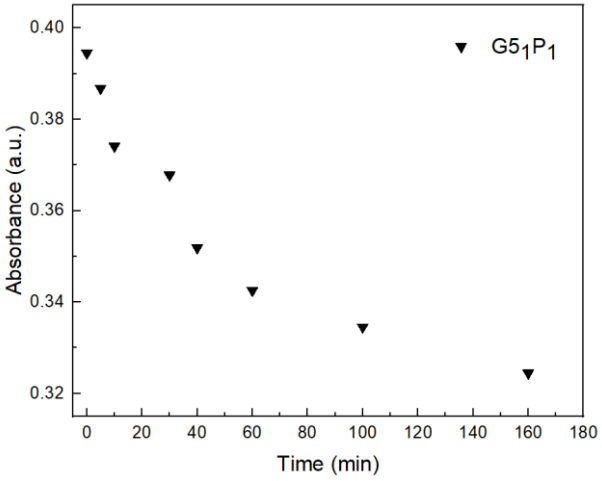

Figure A2: Absorbance versus time (min) graph of MO during the adsorption experiment with the nanocomposite $G5_1P_1$

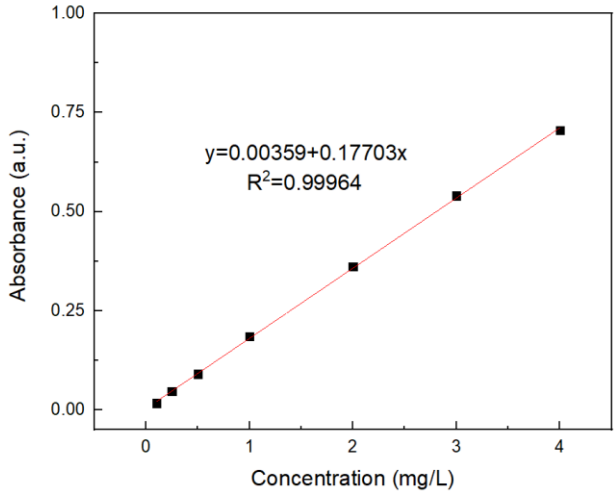

Figure A3: Calibration curve of BF

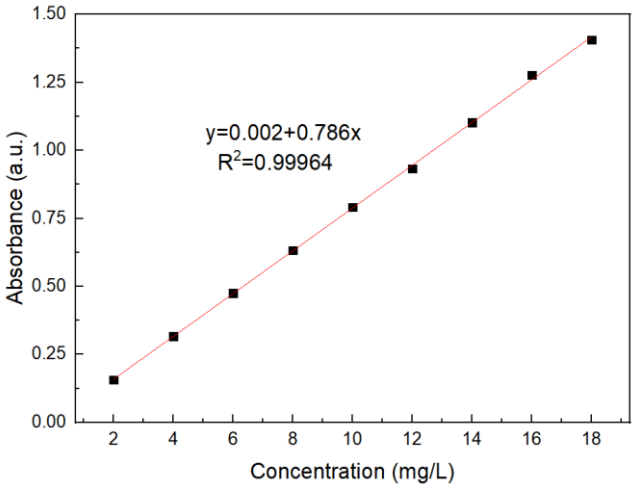

Figure A4: Calibration curve of MO

Preparation of Nanocomposites

The amount of chemicals used is reported in the section of synthesis of nanocomposites (Table 2). In order to synthesize $G3_1P_1$, 0,016 g of PAMAM(G3) containing $7.42x10^{-5}$ mol of $-NH_2$ groups and 0.048 g of Fe_3O_4/P(NIPAM-*co*-MAA) microspheres which contains $7.07x10^{-5}$ mol of -COOH groups were reacted in the system. This means that if $-NH_2$ and -COOH groups reacted totally, there are no free $-NH_2$ and -COOH groups in the nanocomposite (See the following calculations for PAMAM (G3)).

For NH_2 estimation in PAMAM (G3):

$$n = \frac{m}{MW} = \frac{0.016\ g\ of\ PAMAM(G3)}{6909\ g/mol} = 2.31 * 10^{-6}\ mol\ of\ PAMAM(G3)$$

$$2.32 * 10^{-6} x32 = 7.424 * 10^{-5}\ mol\ of - NH_2$$

For the -COOH groups estimation in the Fe_3O_4/P(NIPAM-*co*-MAA) microspheres, it has to be considered that in each microspheres synthesis, 0.2 g of microspheres are obtained. In order to prepare this quantity, 0.025 g of MAA are used; for the nanocomposite synthesis, 0.048 g of microspheres are used. Therefore, we can estimate the –COOH groups in the Fe_3O_4/P(NIPAM-*co*-MAA) polymer as following:

$$n_{COOH} = n_{MAA} = \frac{n}{MW} = \frac{0.025375\ g\ of\ MAA}{86.06\ g/mol} = 2.974 * 10^{-4}\ mol$$

$$n = \frac{0.048\ g\ of\ polymeric\ microspheres}{0.2\ g\ of\ polymeric\ microspheres} * 2.947 * 10^{-4} = 7.07 * 10^{-5}\ mol\ of - COOH$$

For the synthesis of $G4_1P_1$, 0.008 g of the 4th generation of PAMAM which containing 3.60 x 10^{-5} mol of -NH_2 group and 0.024 g of microspheres having 3.53 x 10^{-5} mol of -COOH group were reacted in the experiment (See following calculations).

$$n = \frac{m}{MW} = \frac{0.008\ g\ of\ PAMAM(G4)}{14215\ g/mol} = 5.62 * 10^{-7}\ mol\ of\ PAMAM(G4)$$

$$5.62 * 10^{-7} x64 = 3.60 * 10^{-5}\ mol\ of - NH_2$$

$$n = \frac{0.024\ g\ of\ polymeric\ microspheres}{0.2\ g\ of\ polymeric\ microspheres} * 2.947 * 10^{-4} = 3.53 * 10^{-5}\ mol\ of - COOH$$

In order to synthesize $G5_1P_1$, 0.008 of PAMAM (G5) possessing 3.53*10^{-5} mol of -NH_2 group and 0.024 g of polymer including 3.53 x 10^{-5} mol of -COOH group were reacted in the system (See following calculations).

$$n = \frac{m}{MW} = \frac{0.008\ g\ of\ PAMAM(G5)}{28954\ g/mol} = 2.76 * 10^{-7}\ mol\ of\ PAMAM(G5)$$

$$2.76 * 10^{-7} x128 = 3.53 * 10^{-5}\ mol\ of - NH_2$$

$$n = \frac{0.024\ g\ of\ polymeric\ microspheres}{0.2\ g\ of\ polymeric\ microspheres} * 2.947 * 10^{-4} = 3.53 * 10^{-5}\ mol\ of - COOH$$

Because PAMAM (G5) gave the most promising results in the adsorption of MO and BF dyes, different couplings with the Fe_3O_4/P(NIPAM-*co*-MAA) microspheres were performed by changing the molar ratio of the amino group in PAMAM dendrimer to carboxylic group in the Fe_3O_4/P(NIPAM-*co*-MAA) nanocomposites. Firstly, a molar ratio of amino groups: carboxylic

groups of 1:0.5 was used to synthesize the $G5_1P_{05}$ nanocomposite. For the synthesis of $G5_1P_{05}$, 0.016 g of PAMAM(G5), containing $7.07x10^{-5}$ mol of $-NH_2$ group and 0.024 g of microspheres having $3.53*10^{-5}$ mol of –COOH were used to synthesize the nanocomposites (See following calculations).

$$n = \frac{m}{MW} = \frac{0.016\ g\ of\ PAMAM(G5)}{28954 \frac{g}{mol}} = 5.52 * 10^{-7}\ mol\ of\ PAMAM(G5)$$

$$5.52 * 10^{-7} x128 = 7.07 * 10^{-5}\ mol\ of -NH_2$$

$$n = \frac{0.024\ g\ of\ polymeric\ microspheres}{0.2\ g\ of\ polymeric\ microspheres} * 2.947 * 10^{-4} = 3.53 * 10^{-5}\ mol\ of - COOH$$

Then, a molar ratio of amino groups: carboxylic groups of 1:0.8 was used to synthesize the $G5_1P_{08}$ nanocomposite. In order to perform this coupling, 0.016 g of PAMAM(G5) containing $7.07\ x10^{-5}$ mol of $-NH_2$ group and 0.0384 mg of microspheres having $5.70\ x\ 10^{-5}$ of –COOH were used to synthesize the nanocomposites (See following calculations).

$$n = \frac{m}{MW} = \frac{0.016\ g\ of\ PAMAM(G5)}{28954 \frac{g}{mol}} = 5.52 * 10^{-7}\ mol\ of\ PAMAM(G5)$$

$$5.52 * 10^{-7} x128 = 7.07 * 10^{-5}\ mol\ of -NH_2$$

$$n = \frac{0.0384\ g\ of\ polymeric\ microspheres}{0.2\ g\ of\ polymeric\ microspheres} * 2.947 * 10^{-4} = 5.70 * 10^{-5}\ mol\ of - COOH$$

Pest-OE/UID/QUI/00674/2013

M1420-01-0145-FEDER-000005

Centro de Química da Madeira - CQM⁺ (Madeira 14-20 Program).

Co-financed by: